The linear stability of a drop of fluid during spin coating or subject to a jet of air

I. S. McKinley and S. K. Wilson*

Department of Mathematics, University of Strathclyde,

Livingstone Tower, 26 Richmond Street,

Glasgow G1 1XH, United Kingdom.

(7th February 2001, revised 2nd August 2001)

Abstract

In this paper we investigate the linear stability of an initially axisymmetric thin drop of Newtonian fluid either on a uniformly rotating substrate (the simplest model for spin coating) or on a stationary substrate under the influence of a jet of air directed normally towards the substrate. Drops both with and without a dry patch at their centre are considered. For each problem we examine both the special case of quasi-static motion (corresponding to zero capillary number) analytically and the general case of non-zero capillary number numerically. In all cases the drop is found to be unconditionally unstable, but the growth rate and wavenumber of the most unstable mode depend on the details of the specific problem considered.

---

*Corresponding author. Telephone + 44 (0)141 548 3820, Fax + 44 (0)141 552 8657, Email s.k.wilson@strath.ac.uk

I. INTRODUCTION

The importance of coating processes in many industrial situations has motivated considerable theoretical and experimental work on the spreading of a thin fluid film on a solid substrate (see, for example, the review articles by Oron *et al.*[1], Myers[2] and Davis[3]). Much of this work involves examining the spreading of a fluid subject to an external force. Examples of such forces include gravitational, electrostatic, magnetic and centrifugal forces as well as a non-uniform pressure loading caused by a fluid overlying the thin film. In the present work we shall consider two problems of this type, namely a thin drop of fluid on a uniformly rotating substrate (the simplest model for spin coating) or on a stationary substrate under the influence of a jet of air directed normally towards the substrate. A detailed discussion of the earlier work on both of these problems is given in the recent papers by McKinley *et al.*[4] (hereafter referred to as 'I') and McKinley and Wilson[5] (hereafter referred to as 'II') and hence is not repeated here for brevity. Further discussion of spin coating is given by Larson and Rehg[6] and in the recent paper by Wilson *et al.*[7].

In I McKinley *et al.* considered the unsteady spreading of a thin drop of Newtonian fluid on a horizontal substrate due to a jet of air directed normally towards the substrate. Both planar two-dimensional and axisymmetric three-dimensional problems were solved in the quasi-static limit of small capillary number. Both "annular" drops (i.e. drops with a dry patch at their centre) and "non-annular" drops (i.e. drops without a dry patch) were considered. As in the present work, their results for the axisymmetric case also apply directly to the spin-coating problem with an appropriate redefinition of parameters. In II McKinley and Wilson extended this work to investigate the linear stability of an initially two-dimensional thin ridge of Newtonian fluid of finite width on a planar substrate under the influence of a symmetric two-dimensional jet of air. Again both annular and non-annular ridges were considered. For both problems the special case of quasi-static motion (corresponding to zero capillary number) was examined analytically and the general case of non-zero capillary number was examined numerically. In all cases the ridge was found to

be unconditionally unstable, but the nature and location of the most unstable mode were found to depend on the specific problem considered. In particular, they found that the quasi-static analysis of the non-annular case in I was incomplete. They also found that in the non-annular case (but not in the annular case) the wavenumber of the most unstable mode can jump discontinuously between zero and non-zero values as the size of the ridge is varied. The present work complements I by providing the corresponding analysis of the linear stability of an initially axisymmetric thin drop of Newtonian fluid either on a uniformly rotating substrate or on a stationary substrate under the influence of an axisymmetric jet of air directed normally towards the substrate. Both annular and non-annular drops are considered. For both problems we confirm and extend the analytical results of I in the special case of axisymmetric quasi-static motion (zero capillary number) and investigate numerically the general case of non-zero capillary number.

II. NON-ANNULAR DROPS

A. Problem Formulation

Consider a non-annular drop of incompressible Newtonian fluid with constant viscosity μ, density ρ and surface tension τ on a solid horizontal planar substrate in the presence of a jet of air. We employ cylindrical polar coordinates (r, φ, z), chosen so that the substrate is given by $z = 0$, the thickness of the drop is denoted by $z = h(r, \varphi, t)$ and the velocity of the fluid is denoted by $\mathbf{u} = \mathbf{u}(r, \varphi, z, t)$, where t denotes time. The position of the contact line is denoted by $r = R(\varphi, t)$ at which the contact angle is $\theta = \theta(\varphi, t)$. We model the jet with a parabolic pressure distribution in the air given by $p = p_0 - kr^2/2$, where p denotes the pressure, p_0 is the maximum value of the air pressure at $r = 0$ and k is a positive constant. The shear stress at the free surface caused by the jet is neglected. Acceleration due to gravity is denoted by g. The geometry of the non-annular problem is shown in Fig. 1.

We follow the approach adopted in I and II and assume that the speed of the contact

line is related to the contact angle by the "Tanner law" $R_t = \kappa(\theta^m - \theta_0^m)$, where θ_0 is the equilibrium contact angle and κ is an empirically determined positive constant with dimensions of velocity. More general Tanner laws were used in I.

Hereafter all quantities are non-dimensionalised as in I and II using a characteristic radial length scale L (to be defined subsequently) and κ as the characteristic horizontal velocity scale.

Provided that inertia effects are negligible and that the drop is sufficiently thin, the familiar lubrication approximation to the governing Navier-Stokes and mass conservation equations together with the appropriate boundary conditions representing continuity of normal and tangential stress and the kinematic condition at the free surface together with Navier slip with (small) positive slip coefficient λ at the substrate yield the governing equation for h, namely

$$Ch_t + \nabla \cdot \left[h^2 \left(\frac{h}{3} + \lambda \right) \nabla \left(\nabla^2 h - G^2 h + \frac{Jr^2}{2} \right) \right] = 0. \tag{1}$$

Equation (1) must be solved together with the Tanner law

$$R_t = \theta^m - 1. \tag{2}$$

The constant $J = kL^3/\tau\theta_0$ is a non-dimensional measure of the jet strength, $C = \kappa\mu/\tau\theta_0^3$ is the capillary number and $G^2 = \rho g L^2/\tau$ is the Bond number. Without loss of generality we can choose $L = (\tau\theta_0/k)^{1/3}$ (corresponding to setting $J = 1$). For clarity we shall retain J explicitly in all of our analytical calculations but set $J = 1$ in all of our numerical calculations.

The appropriate boundary conditions for Eq. (1) are that the free surface has zero height and prescribed contact angle at the contact line,

$$h(R, \varphi, t) = 0, \tag{3}$$

$$\left(h_r - \frac{1}{R^2} R_\varphi h_\varphi \right) \left(1 + \frac{R_\varphi^2}{R^2} \right)^{-1/2} \Bigg|_{r=R} = -\theta, \tag{4}$$

together with the regularity conditions

$$h_r(0,\varphi,t) = 0, \tag{5}$$

$$Q(0,\varphi,t) = 0, \tag{6}$$

where

$$Q = \int_0^h u\,\mathrm{d}z \tag{7}$$

is the flux in the r direction, which must be satisfied together with appropriate initial conditions for h and R. The volume of the drop is given by

$$2\pi V = \int_0^{2\pi}\int_0^R hr\,\mathrm{d}r\mathrm{d}\varphi. \tag{8}$$

Note that if we identify the dimensional jet strength k with $\rho\omega^2$ then Eq. (1) is identical to the equation describing the spin coating of a thin drop on a horizontal substrate rotating with constant angular speed ω (see Moriarty *et al.*[8] and I). Hence all the results presented here apply to both spin-coating and air-jet-blowing problems.

For simplicity we shall hereafter restrict our attention to the special case of sufficiently small drops in which gravity effects are negligible, and hence set $G = 0$. In addition, we follow II and adopt the linear Tanner law obtained by setting $m = 1$ in Eq. (2).

B. Basic State

In equilibrium $h(r,\varphi,t) = h_0(r)$, $R(\varphi,t) = R_0$ and $\theta = 1$. Substituting these expressions into Eqs (1) and (3) – (5) and using Eq. (6) with $G = 0$ yields the governing equation for the basic-state profile, namely

$$h_0''' + \frac{1}{r}h_0'' - \frac{1}{r^2}h_0 + Jr = 0, \tag{9}$$

where the prime denotes differentiation with respect to r, subject to the boundary conditions $h_0(R_0) = 0$, $h_0'(R_0) = -1$ and $h_0'(0) = 0$. The solution for h_0 is given by

$$h_0 = \frac{1}{32}(r^2 - R_0^2)\left[JR_0(R_0^2 - r^2) - 16\right], \tag{10}$$

and from Eq. (8) the volume of the drop is given by

$$V = \frac{1}{192} R_0^3 (24 - J R_0^3). \tag{11}$$

Figure 2 plots the basic-state profiles for $R_0 = 1$, 1.5, 2 and 2.5. These solutions are exactly the axisymmetric non-annular solutions described in I. Note that "physical" solutions (i.e. solutions for which $h_0 \geq 0$ over the entire interval $0 \leq r \leq R_0$) exist only when R_0 lies in the range $0 \leq R_0 \leq (16/J)^{1/3}$.

C. Linear Stability Problem

We analyse the linear stability of the drop to small perturbations with azimuthal wavenumber $q \geq 0$ by seeking solutions in the form $h = h_0(r) + h_1(r) \exp(iq\varphi + \sigma t)$ and $R = R_0 + R_1 \exp(iq\varphi + \sigma t)$, where $h_1(r)$ is the perturbation to the basic-state profile, R_1 is the perturbation to the position of the contact line and σ is the unknown (complex) growth coefficient. Note that the wavenumber q must be an integer to ensure physically sensible solutions. Substituting these expressions into Eqs (1) – (6) and retaining only first-order terms in the perturbations yields the governing equation for h_1:

$$\begin{aligned} C\sigma h_1 + \frac{1}{r}\left[r h_0^2 \left(\frac{h_0}{3} + \lambda \right) \left(h_1'' + \frac{1}{r} h_1' - \frac{q^2}{r^2} h_1 \right)' \right]' \\ - \frac{q^2}{r^2} h_0^2 \left(\frac{h_0}{3} + \lambda \right) \left(h_1'' + \frac{1}{r} h_1' - \frac{q^2}{r^2} h_1 \right) = 0, \end{aligned} \tag{12}$$

which is subject to the boundary conditions

$$R_1 = h_1(\pm R_0), \tag{13}$$

$$h_1'(\pm R_0) \pm h_0''(\pm R_0) R_1 = \mp \sigma R_1. \tag{14}$$

Eliminating R_1 from Eqs (13) and (14) and using Eq. (10) yields

$$h_1'(\mp R_0) \pm \left(\frac{J R_0^3 + 4}{4 R_0} \right) h_1(\mp R_0) = \pm \sigma h_1(\mp R_0). \tag{15}$$

As Hocking and Miksis[9] point out, in the special case $q = 0$ (but not otherwise) it is also necessary to impose the volume condition

$$\int_0^{R_0} h_1 r \, \mathrm{d}r = 0. \tag{16}$$

D. Quasi-static Motion $C = 0$

We can make considerable analytical progress in the special case $C = 0$. In this case the bulk of the drop instantaneously adopts a quasi-static profile whose subsequent motion is entirely determined by the Tanner law given in Eq. (2).

1. Axisymmetric Perturbations $q = 0$

The solution of Eq. (12) for h_1 when $C = 0$ and $q = 0$ that does not have a singularity at $r = R_0$ is

$$h_1 = \alpha r^2 + \beta + \gamma \ln r, \tag{17}$$

where α, β and γ are constants. For solutions that are bounded at the origin we require $\gamma = 0$. Using the boundary condition (15) and the volume condition (16) yields $\sigma = \sigma_0$, where

$$\sigma_0 = \frac{JR_0^3 - 12}{4R_0}, \tag{18}$$

recovering the conditionally stable growth rate first obtained in I.

2. Non-axisymmetric Perturbations $q \geq 1$

A solution of Eq. (12) for h_1 when $C = 0$ and $q \geq 1$ that does not have a singularity at $r = R_0$ is

$$h_1 = \alpha r^q + \frac{\beta}{r^q}, \tag{19}$$

where α and β are constants. For solutions that are bounded at the origin we require $\beta = 0$, and using the boundary condition (15) yields $\sigma = \sigma_q$, where

$$\sigma_q = \frac{JR_0^3 + 4(1-q)}{4R_0}, \tag{20}$$

for $q = 1, 2, 3, \ldots$. Note that, because these solutions do not satisfy the volume condition (16), substituting $q = 0$ into Eq. (20) does not recover the expression obtained previously for σ_0. The neutral stability curves are obtained by setting $\sigma_q = 0$ in Eq. (20) and are given by

$$R_0 = \left(\frac{4(q-1)}{J}\right)^{1/3}, \tag{21}$$

for $q = 1, 2, 3, \ldots$.

3. General Perturbations $q \geq 0$

Figure 3 plots the growth rate σ_q as a function of R_0 for $q = 0, 1, 2, \ldots, 7$. Since the largest eigenvalue is $\sigma_1 = JR_0^2/4 > 0$ the drop is unconditionally unstable via the $q = 1$ mode. Note that from Eqs (18) and (20) we have $\sigma_0 = \sigma_4$, and so both $q = 0$ and $q = 4$ modes correspond to exactly the same curve in Fig. 3. Furthermore, the neutral stability curve for $q = 5$ is identical to the curve where the basic-state solutions become unphysical, namely $R_0 = (16/J)^{1/3}$. For $q \geq 5$ Fig. 3 shows that $\sigma_q < 0$ for all values of R_0 corresponding to physical solutions, and hence that these modes are always stable.

E. The General Case $C \neq 0$

In the general case $C \neq 0$ the bulk of the drop responds on a time scale of C and so the motion is always retarded relative to the case $C = 0$. To obtain the neutral stability curves for $C \neq 0$ we set $\sigma = 0$ in Eq. (12) and the boundary conditions (15). This procedure yields the same neutral stability curves as those calculated previously in the case $C = 0$.

1. Numerical Procedure

A FORTRAN code was written to solve the eigenvalue problem given by Eq. (12) and the boundary conditions (15) numerically using finite differences. The details of this numerical procedure are given by McKinley[10] and in II. In all the calculations that follow we set $N = 201$, where $N+1$ is the number of grid points, and the slip coefficient is set to $\lambda = 0.01$. The value of λ was chosen to be reasonably small, but not so small as to cause numerical difficulties. The work of Hocking & Miksis[9] suggests that the results will be qualitatively similar for other (small) values of λ. Choosing N to be an odd number ensures that $r = 0$ is not a grid point.

2. Results

Figure 4 plots the largest eigenvalue σ as a function of R_0 for $q = 0, 1, 2, \ldots, 6$ in the case $C = 1$. The neutral stability points are given by $R_0 = (12/J)^{1/3}$ for the $q = 0$ mode, and by Eq. (21) for the $q \geq 1$ modes. For R_0 in the range $0 < R_0 < 2.12$ the most unstable mode corresponds to $q = 1$, while for $2.12 < R_0 < 2.46$ it corresponds to $q = 2$ and for $2.46 < R_0 \leq (16/J)^{1/3} \approx 2.52$ to $q = 3$. Note that, unlike in the case $C = 0$ in which they are identical, for $C \neq 0$ the curves corresponding to the $q = 0$ and $q = 4$ modes coincide only at $\sigma = 0$.

Figures 5(a) and (b) plot the largest eigenvalue σ as a function of R_0 for $q = 0, 1, 2, \ldots, 7$ for $C = 0.1$ and 0.001 respectively. The thick curves correspond to the solutions in the special case $C = 0$ given by σ_q for $q = 0, 1, 2, \ldots, 7$. For $C = 0.1$ (Fig. 5(a)) the most unstable mode corresponds to $q = 1$ for $0 < R_0 < 2.19$ and to $q = 2$ for $2.19 < R_0 < 2.52$. For $C = 0.01$ (not shown) the same qualitative behaviour occurs; however the value of R_0 at which the most unstable mode changes from the $q = 1$ mode to the $q = 2$ mode is $R_0 \approx 2.38$. For $C = 0.001$ (Fig. 5(b)) the most unstable mode corresponds to $q = 1$ for all values of R_0 corresponding to physical solutions. Figure 5 shows that the effect of decreasing C towards

zero is to increase the growth rate of the most unstable mode. In particular, Fig. 5 shows how the numerically calculated values of σ approach σ_q in the limit $C \to 0$.

III. ANNULAR DROPS

A. Problem Formulation

Clearly, the major difference between the annular drops discussed in this section and the non-annular drops discussed in the previous section is that the former have two contact lines and hence two contact angles. The (dimensional) positions of the "inner" and "outer" contact lines are denoted by $r = R_1(\varphi, t)$ at which the contact angle is $\phi = \phi(\varphi, t)$ and $r = R_2(\varphi, t)(> R_1)$ at which the contact angle is $\theta = \theta(\varphi, t)$, respectively. The geometry of the annular problem is shown in Fig. 6.

Since there are now two moving contact lines, we need two Tanner laws relating the speed of each contact line to its contact angle. These are given (in dimensional variables) by $(R_1)_t = \kappa(\phi_0^m - \phi^m)$ and $(R_2)_t = \kappa(\theta^m - \theta_0^m)$, where ϕ_0 and θ_0 are the (possibly different) equilibrium values of the inner and outer contact angles respectively.

Non-dimensionalising as in the non-annular case the governing equation for h is again given by Eq. (1) which must be solved together with the Tanner laws

$$(R_1)_t = \phi_0^m - \phi^m, \tag{22}$$

$$(R_2)_t = \theta^m - 1. \tag{23}$$

The appropriate boundary conditions for Eq. (1) in this case are

$$h(R_1, \varphi, t) = 0, \tag{24}$$

$$h(R_2, \varphi, t) = 0, \tag{25}$$

$$\left(h_r - \frac{1}{R_1^2}(R_1)_\varphi h_\varphi\right)\left(1 + \frac{(R_1)_\varphi^2}{R_1^2}\right)^{-1/2}\Bigg|_{r=R_1} = \phi, \tag{26}$$

$$\left(h_r - \frac{1}{R_2^2}(R_2)_\varphi h_\varphi\right)\left(1 + \frac{(R_2)_\varphi^2}{R_2^2}\right)^{-1/2}\Bigg|_{r=R_2} = -\theta, \tag{27}$$

which must be satisfied together with appropriate initial conditions for h, R_1 and R_2. The volume of the annular drop is given by

$$2\pi V = \int_0^{2\pi} \int_{R_1}^{R_2} hr \, \mathrm{d}r\mathrm{d}\varphi. \tag{28}$$

As in the non-annular case, we shall restrict our attention to the special case $G = 0$ and set $m = 1$ in Eqs (22) and (23).

B. Basic State

In equilibrium $h(r, \varphi, t) = h_0(r)$, $R_1(\varphi, t) = R_1^0$, $R_2(\varphi, t) = R_2^0$, $\theta = 1$ and $\phi = \phi_0$. Substituting these expressions into Eqs (1), (24), (25) and (27) with $G = 0$ reveals that the governing equation for the basic-state profile is Eq. (9) subject to the boundary conditions $h_0(R_1^0) = 0$, $h_0(R_2^0) = 0$ and $h_0'(R_2^0) = -1$. The solution for h_0 is given by

$$h_0 = f(r, R_1^0, R_2^0) + Jg(r, R_1^0, R_2^0), \tag{29}$$

and from Eq. (28) the volume of the drop is given by

$$V = S(R_1^0, R_2^0) + JT(R_1^0, R_2^0), \tag{30}$$

where the functions $f(r, R_1^0, R_2^0)$, $g(r, R_1^0, R_2^0)$, $S = S(R_1^0, R_2^0)$ and $T = T(R_1^0, R_2^0)$ are given by Eqs (47), (48), (51) and (52) in I respectively and hence are not reproduced here for brevity. The remaining boundary condition (26) yields the relationship between ϕ_0, R_1^0 and R_2^0, which is given explicitly by Eq. (54) in I. Figure 7 plots the basic-state profiles for $R_2^0 = 2$, 2.3, 2.6 and 2.9 in the case $\phi_0 = 1$. These solutions are exactly the axisymmetric annular solutions described in I. For $\phi_0 \leq 1$ solutions exist only for values of R_2^0 greater than a critical value, while for $\phi_0 > 1$ solutions exist only for values of R_1^0 less than a critical value. This behaviour is shown in Fig. 8 which plots R_1^0 against the corresponding value for R_2^0 in the cases $\phi_0 = 0.7$, 1 and 1.3.

C. Linear Stability Problem

To analyse the linear stability of the drop we perturb h as before and seek solutions in the form $R_1 = R_1^0 + R_1^1 \exp(iq\varphi + \sigma t)$ and $R_2 = R_2^0 + R_2^1 \exp(iq\varphi + \sigma t)$, where R_1^1 and R_2^1 are the perturbations to the positions of the contact lines. Substituting these expressions into Eqs (1) and (22) – (27) reveals that the governing equation for h_1 is Eq. (12) subject to the boundary conditions

$$R_1^1 = -\frac{1}{\phi_0} h_1(R_1^0), \tag{31}$$

$$R_2^1 = h_1(R_2^0), \tag{32}$$

$$h_1'(R_1^0) + h_0''(R_1^0) R_1^1 = -\sigma R_1^1, \tag{33}$$

$$h_1'(R_2^0) + h_0''(R_2^0) R_2^1 = -\sigma R_2^1. \tag{34}$$

Eliminating R_1^1 and R_2^1 from Eqs (31) – (34) and using Eq. (29) yields

$$\phi_0 h_1'(R_1^0) - f_1(J, R_1^0, R_2^0) h_1(R_1^0) = \sigma h_1(R_1^0), \tag{35}$$

$$h_1'(R_2^0) + f_2(J, R_1^0, R_2^0) h_1(R_2^0) = -\sigma h_1(R_2^0), \tag{36}$$

where the functions $f_1(J, R_1^0, R_2^0)$ and $f_2(J, R_1^0, R_2^0)$ are given by

$$\begin{aligned} f_1(J, R_1^0, R_2^0) = \Big\{ & 4(R_1^0)^2 R_2^0 [3JR_2^0((R_1^0)^2 - (R_2^0)^2) + 8] \ln(R_1^0/R_2^0) \\ & -[(R_1^0)^2 - (R_2^0)^2][5J(R_1^0)^4 - 2J(R_1^0)^2(R_2^0)^2 + J(R_2^0)^4 - 16R_2^0] \Big\} \\ & \times \Big\{ 16(R_1^0)^2 [(R_1^0)^2 - (R_2^0)^2 - 2(R_2^0)^2 \ln(R_1^0/R_2^0)] \Big\}^{-1}, \end{aligned} \tag{37}$$

$$\begin{aligned} f_2(J, R_1^0, R_2^0) = & \Big\{ 4(R_2^0)^2 [J(R_2^0)^3 + 4] \ln(R_1^0/R_2^0) + [(R_1^0)^2 - (R_2^0)^2] \\ & \times [JR_2^0((R_1^0)^2 - (R_2^0)^2) + 8] \Big\} \Big\{ 8R_2^0 [(R_1^0)^2 - (R_2^0)^2 - 2(R_2^0)^2 \ln(R_1^0/R_2^0)] \Big\}^{-1}. \end{aligned} \tag{38}$$

Again in the special case $q = 0$ it is also necessary to impose the volume condition

$$\int_{R_1^0}^{R_2^0} h_1 r \, \mathrm{d}r = 0. \tag{39}$$

D. Quasi-static Motion $C = 0$

1. Axisymmetric Perturbations $q = 0$

From Sec. II D 1 the solution for h_1 when $C = 0$ and $q = 0$ is given by Eq. (17). Applying the boundary conditions (35) and (36) and the volume condition (39) recovers the unconditionally unstable results first obtained in I, namely $\sigma = \sigma_{0+} > 0$ and $\sigma = \sigma_{0-} < \sigma_{0+}$. The expressions for $\sigma_{0\pm}$ are not repeated here for brevity. Figure 9 plots σ_{0+} as a function of R_2^0 for $\phi_0 = 0.7$, 1 and 1.3. Recall that R_1^0 is not constant on each of these curves, but varies with R_2^0 as shown in Fig. 8.

2. Non-axisymmetric Perturbations $q \geq 1$

From Sec. II D 2 the solution for h_1 when $C = 0$ and $q \geq 1$ is given by Eq. (19) subject to the boundary conditions (35) and (36). Solving this system yields two expressions for σ, namely $\sigma = \sigma_{q+} > 0$ and $\sigma = \sigma_{q-} < \sigma_{q+}$. The expressions for $\sigma_{q\pm}$ are not given here for brevity. As before note that, because these solutions do not satisfy the volume condition (39), substituting $q = 0$ into $\sigma_{q\pm}$ does not recover the expressions obtained previously for $\sigma_{0\pm}$.

3. General Perturbations $q \geq 0$

Figures 10(a) – (c) plot the growth rate σ_{q+} as a function of R_2^0 for $q = 0$, 1, 2, 3 and 4 in the cases $\phi_0 = 0.7$, 1 and 1.3 respectively. Again recall that R_1^0 is not constant on each of these curves, but varies with R_2^0 as shown in Fig. 8.

For $\phi_0 = 0.7$ (Fig. 10(a)) the most unstable mode corresponds to $q = 0$ for $0 < R_1^0 < 0.19$ and $q = 1$ for $R_1^0 > 0.19$. For $\phi_0 = 1$ (Fig. 10(b)) the same qualitative behaviour occurs with the most unstable mode corresponding to $q = 0$ for $0 < R_1^0 < 0.26$ and $q = 1$ for $R_1^0 > 0.26$. For $\phi_0 = 1.3$ (Fig. 10(c)), however, the most unstable mode corresponds to $q = 1$

for $0 < R_2^0 < 1.86$ and to $q = 0$ for $1.86 < R_2^0 < 2.52$. These results are summarised in Fig. 11, which shows the wavenumber of the most unstable mode for $\phi_0 = 0.7$, 1 and 1.3. The dots on Fig. 11 denote the values of R_1^0 and R_2^0 at which the most unstable mode jumps between $q = 0$ and $q = 1$.

E. The General Case $C \neq 0$

Figures 12(a) and (b) plot the largest eigenvalue σ as a function of R_2^0 for $q = 0$, 1, 2, ..., 9 in the case $\phi_0 = 0.7$ for $C = 1$ and 0.001 respectively. For $C = 1$ (Fig. 12(a)) the most unstable mode corresponds to $q = 0$ for small values of R_1^0. As R_1^0 increases the most unstable mode jumps from $q = 0$ to $q = 2$ then to $q = 3$, $q = 4$ and so on. The same qualitative behaviour occurs for $C = 0.1$ and $C = 0.01$ (not shown). For $C = 0.001$ (Fig. 12(b)) the most unstable mode corresponds to $q = 0$ for small values of R_1^0. As R_1^0 increases the most unstable mode jumps from $q = 0$ to $q = 1$ then to $q = 2$, $q = 3$ and so on.

Figures 13(a) and (b) plot the largest eigenvalue σ as a function of R_2^0 for $q = 0$, 1, 2, ..., 9 in the case $\phi_0 = 1$ for $C = 1$ and 0.001 respectively. For $C = 1$ (Fig. 13(a)) the most unstable mode corresponds to $q = 0$ for small values of R_1^0. As R_1^0 increases the most unstable mode jumps from $q = 0$ to $q = 2$ then to $q = 3$, $q = 4$ and so on. The same qualitative behaviour occurs for $C = 0.1$ (not shown). For $C = 0.001$ (Fig. 13(b)) the most unstable mode corresponds to $q = 0$ for small values of R_1^0. As R_1^0 increases the most unstable mode jumps from $q = 0$ to $q = 1$ then to $q = 2$, $q = 3$ and so on. The same qualitative behaviour occurs for $C = 0.01$ (not shown).

Figures 14(a) and (b) plot the largest eigenvalue σ as a function of R_2^0 for $q = 0$, 1, 2, ..., 9 in the case $\phi_0 = 1.3$ for $C = 1$ and 0.001 respectively. For $C = 1$ (Fig. 14(a)) the most unstable mode corresponds to $q = 2$ for small values of R_2^0. As R_2^0 increases the most unstable mode jumps from $q = 2$ to $q = 0$. For $C = 0.1$ (not shown) the most unstable mode jumps from $q = 1$ to $q = 2$ followed by $q = 0$ as R_2^0 increases from zero. For $C = 0.01$ (not shown) the most unstable mode jumps from $q = 1$ to $q = 2$, then to $q = 1$ again followed by

$q = 0$ as R_2^0 increases from zero. For $C = 0.001$ (Fig. 14(b)) the most unstable mode jumps from $q = 1$ for small values of R_2^0 to $q = 0$ as R_2^0 increases from zero.

Figures 12 – 14 show that the effect of decreasing C towards zero is to increase the growth rate of the most unstable mode.

These results are summarised in Figs 15(a) – (d) which show the wavenumber of the most unstable mode corresponding to $\phi_0 = 0.7$, 1 and 1.3 for $C = 1$, 0.1, 0.01 and 0.001. The dots on Fig. 15 denote the values of R_1^0 and R_2^0 at which the most unstable mode jumps between two different values of q.

IV. CONCLUSIONS

In this paper we investigated the linear stability to both axisymmetric ($q = 0$) and non-axisymmetric ($q \neq 0$) perturbations of an initially axisymmetric thin drop of Newtonian fluid either on a rotating substrate or on a stationary substrate under the influence of a jet of air directed normally towards the substrate. Both annular and non-annular drops were considered. For each problem we examined both the special case of quasi-static motion ($C = 0$) analytically and the general case $C \neq 0$ numerically. In all cases the drop was found to be unconditionally unstable, but the growth rate and wavenumber of the most unstable mode depend on the details of the specific problem considered.

First we analysed a non-annular drop. For axisymmetric quasi-static motion the conditionally unstable mode obtained in I was recovered. For general quasi-static motion the drop is always unstable via the $q = 1$ mode. When $C \neq 0$ the drop is always unstable and the growth rate and wavenumber of the most unstable mode depend on the values of R_0 and C. In particular, the most unstable wavenumber increases as R_0 increases and the quasi-static results are recovered in the limit $C \to 0$.

A similar analysis was performed for an annular drop. For axisymmetric quasi-static motion the unconditionally unstable results obtained in I were again recovered. For general quasi-static motion the drop is always unstable via either the $q = 0$ mode or the $q = 1$ mode

depending on the values of R_1^0, R_2^0 and ϕ_0. When $C \neq 0$ the drop is always unstable and, as in the non-annular case, the growth rate and wavenumber of the most unstable mode depend on the values of R_1^0, R_2^0, ϕ_0 and C. For $\phi_0 \leq 1$ the most unstable wavenumber increases as R_1^0 increases, while for $\phi_0 > 1$ the most unstable wavenumber always corresponds to $q = 0$ for large enough R_2^0. Again the quasi-static results are recovered in the limit $C \to 0$.

There are, as far as the authors are aware, no experimental results for either spin coating or air-jet blowing which are directly comparable with the present work. In particular, comparison between experimental measurements of the most unstable wavenumber (and its growth rate) with the predictions of the present theoretical calculations would be of considerable interest.

ACKNOWLEDGEMENTS

During the course of the present work the first author (ISM) was supported by the University of Strathclyde, Glasgow, Scotland, UK, via the Graduate Teaching Assistant Scheme. Both authors wish to thank Professor D. M. Sloan and Dr B. R. Duffy (Department of Mathematics, University of Strathclyde) for invaluable discussions during the course of the present work.

REFERENCES

[1] A. Oron, S. H. Davis, and S. G. Bankoff, "Long-scale evolution of thin liquid films," Rev. Mod. Phys. **69**, 931–980 (1997).

[2] T. G. Myers, "Thin films with high surface tension," SIAM Rev. **40**, 441–462 (1998).

[3] S. H. Davis, "Interfacial fluid dynamics," Chapter 1 in *Perspectives in Fluid Dynamics*, edited by G. K. Batchelor, H. K. Moffatt, and M. G. Worster (Cambridge University Press, Cambridge, 2000), pp. 1–51.

[4] I. S. McKinley, S. K. Wilson, and B. R. Duffy, "Spin coating and air-jet blowing of thin viscous drops," Phys. Fluids **11**, 30–47 (1999).

[5] I. S. McKinley and S. K. Wilson, "The linear stability of a ridge of fluid subject to a jet of air," Phys. Fluids **13**, 872–883 (2001).

[6] R. G. Larson and T. G. Rehg, "Spin Coating," Chapter 14 in *Liquid Film Coating*, edited by S. F. Kistler and P. M. Schweizer (Chapman Hall, London, 1997), pp. 709–734.

[7] S. K. Wilson, R. Hunt, and B. R. Duffy, "The rate of spreading in spin coating," J. Fluid Mech. **413** 65–88 (2000).

[8] J. A. Moriarty, L. W. Schwartz, and E. O. Tuck, "Unsteady spreading of thin liquid films with small surface tension," Phys. Fluids A **3**, 733–742 (1991).

[9] L. M. Hocking and M. J. Miksis, "Stability of a ridge of fluid," J. Fluid Mech. **247**, 157–177 (1993).

[10] I. S. McKinley, "Studies in thin-film flows," Ph. D. Thesis, University of Strathclyde, Glasgow, United Kingdom, 1999.

FIGURE CAPTIONS

FIG. 1: Geometry of the non-annular problem.

FIG. 2: Basic-state profiles of a non-annular drop for $R_0 = 1$, 1.5, 2 and 2.5.

FIG. 3: Plot of the growth rates σ_q for $q = 0, 1, 2, \ldots, 7$ as a function of R_0 for a non-annular drop in the case $C = 0$.

FIG. 4: Plot of the largest eigenvalue σ as a function of R_0 for a non-annular drop for $q = 0$, 1, 2, ..., 6 in the case $C = 1$.

FIG. 5: Plot of the largest eigenvalue σ as a function of R_0 for a non-annular drop for $q = 0, 1, 2, \ldots, 7$ for (a) $C = 0.1$ and (b) $C = 0.001$. The thick curves correspond to the solutions in the special case $C = 0$ given by $\sigma_0 = (JR_0^3 - 12)/4R_0$ for $q = 0$ and $\sigma_q = (JR_0^3 + 4(1-q))/4R_0$ for $q = 1, 2, 3, \ldots, 7$.

FIG. 6: Geometry of the annular problem.

FIG. 7: Basic-state profiles of an annular drop for $R_2^0 = 2$, 2.3, 2.6 and 2.9 in the case $\phi_0 = 1$.

FIG. 8: Plot of R_1^0 against R_2^0 for annular solutions in the cases $\phi_0 = 0.7$, 1 and 1.3.

FIG. 9: Plot of the growth rate σ_{0+} as a function of R_2^0 for an annular drop for $\phi_0 = 0.7$, 1 and 1.3 in the case $q = 0$ and $C = 0$.

FIG. 10: Plot of the growth rates σ_{q+} for $q = 0$, 1, 2, 3 and 4 as a function of R_2^0 for an annular drop in the cases (a) $\phi_0 = 0.7$, (b) $\phi = 1$ and (c) $\phi = 1.3$ for $C = 0$.

FIG. 11: Plot of R_1^0 against R_2^0 for annular solutions corresponding to $\phi_0 = 0.7$, 1 and 1.3 showing the most unstable wavenumber for $C = 0$. The dots correspond to the values of R_1^0 and R_2^0 at which the most unstable mode jumps between $q = 0$ and $q = 1$.

FIG. 12: Plot of the largest eigenvalue σ as a function of R_2^0 for an annular drop for $q = 0$, 1, 2, ..., 9 in the case $\phi_0 = 0.7$ for (a) $C = 1$ and (b) $C = 0.001$.

FIG. 13: Plot of the largest eigenvalue σ as a function of R_2^0 for an annular drop for $q = 0$, 1, 2, ..., 9 in the case $\phi_0 = 1$ for (a) $C = 1$ and (b) $C = 0.001$.

FIG. 14: Plot of the largest eigenvalue σ as a function of R_2^0 for an annular drop for $q = 0$, 1, 2, ..., 9 in the case $\phi_0 = 1.3$ for (a) $C = 1$ and (b) $C = 0.001$.

FIG. 15 (a) – (d): Plot of R_1^0 against R_2^0 for annular solutions corresponding to $\phi_0 = 0.7$, 1 and 1.3 showing the most unstable wavenumber for (a) $C = 1$, (b) $C = 0.1$, (c) $C = 0.01$ and (d) $C = 0.001$. The dots correspond to the values of R_1^0 and R_2^0 at which the most unstable mode jumps between two different values of q.

Figure 1

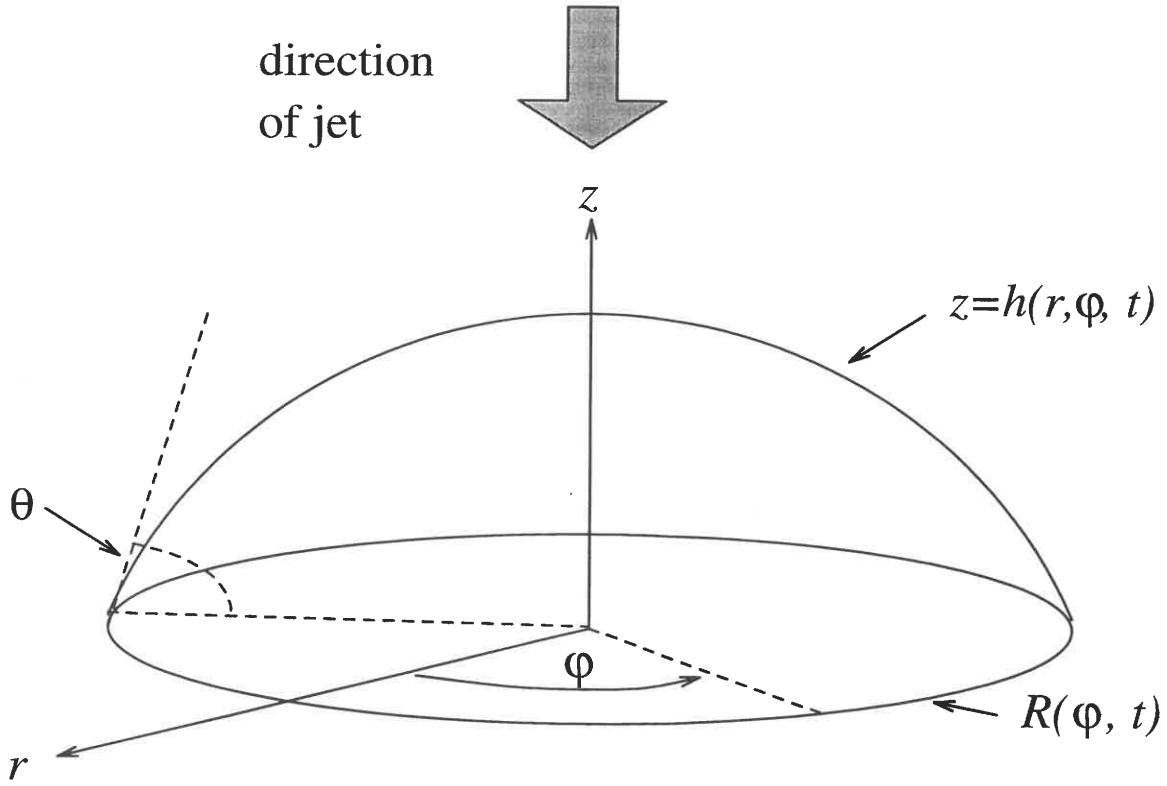

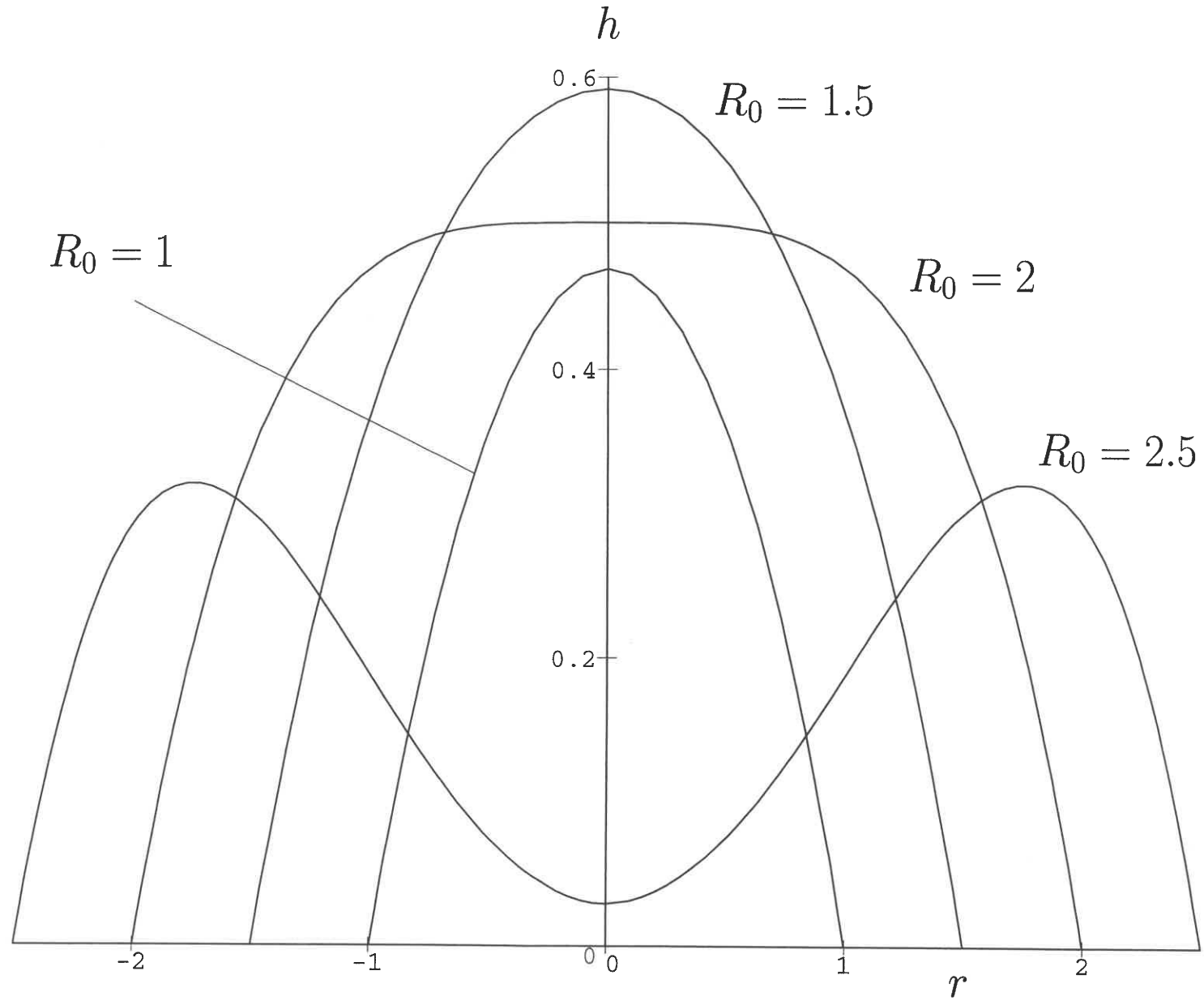
h
0.6
0.4
0.2
0
$R_0 = 1.5$
$R_0 = 1$
$R_0 = 2$
$R_0 = 2.5$
-2
-1
0
1
2
r

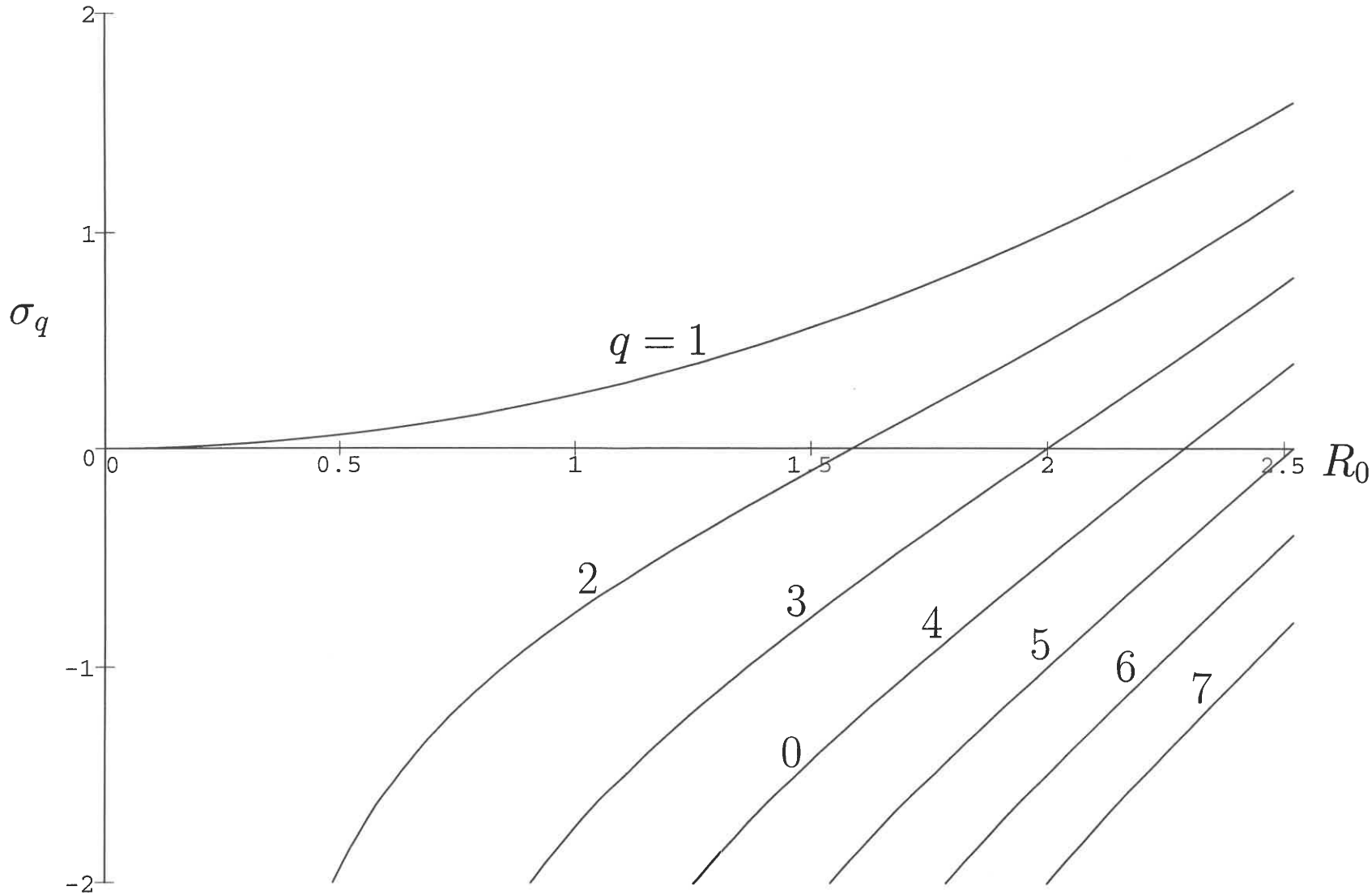
2
1
0
-1
-2
σ_q
0
0.5
1
1.5
2
2.5
R_0
$q = 1$
2
3
4
5
6
7
0

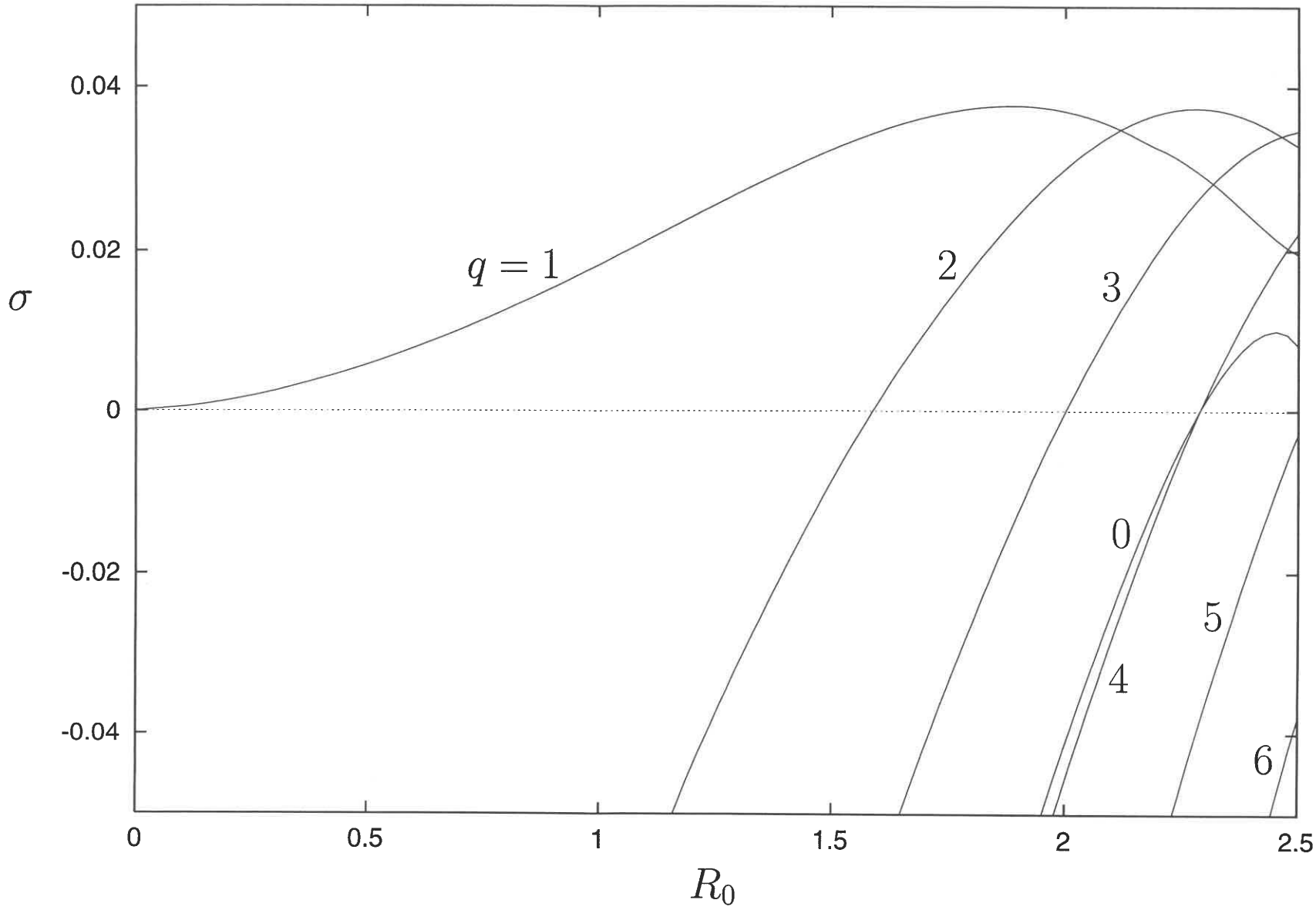
0.04
0.02
0
-0.02
-0.04
σ
$q = 1$
2
3
0
5
4
6
0
0.5
1
1.5
2
2.5
R_0

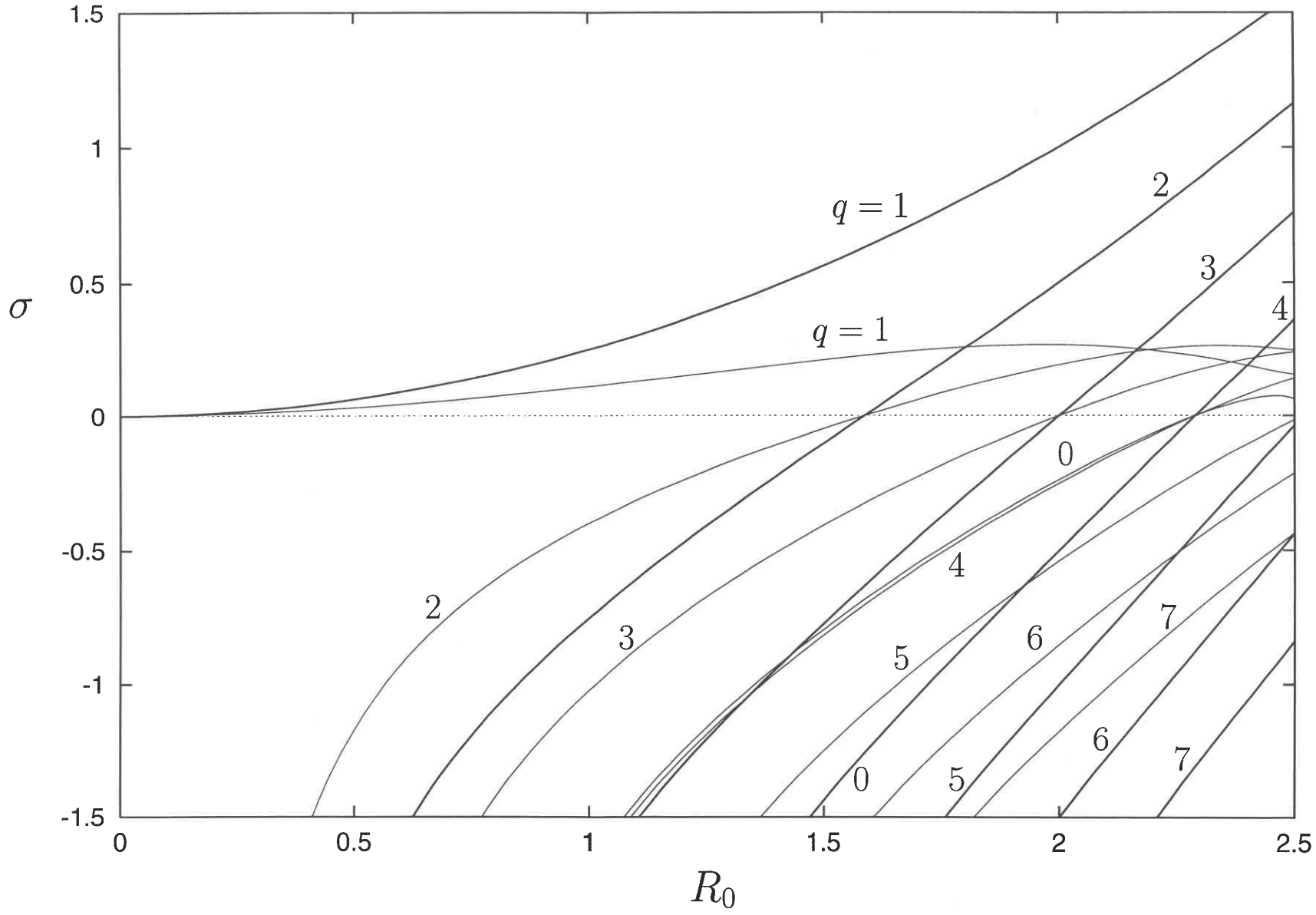
1.5
1
0.5
0
-0.5
-1
-1.5
0
0.5
1
1.5
2
2.5
σ
R_0
$q = 1$
$q = 1$
2
3
4
0
2
3
4
5
6
7
0
5
6
7

Figure 5(b)

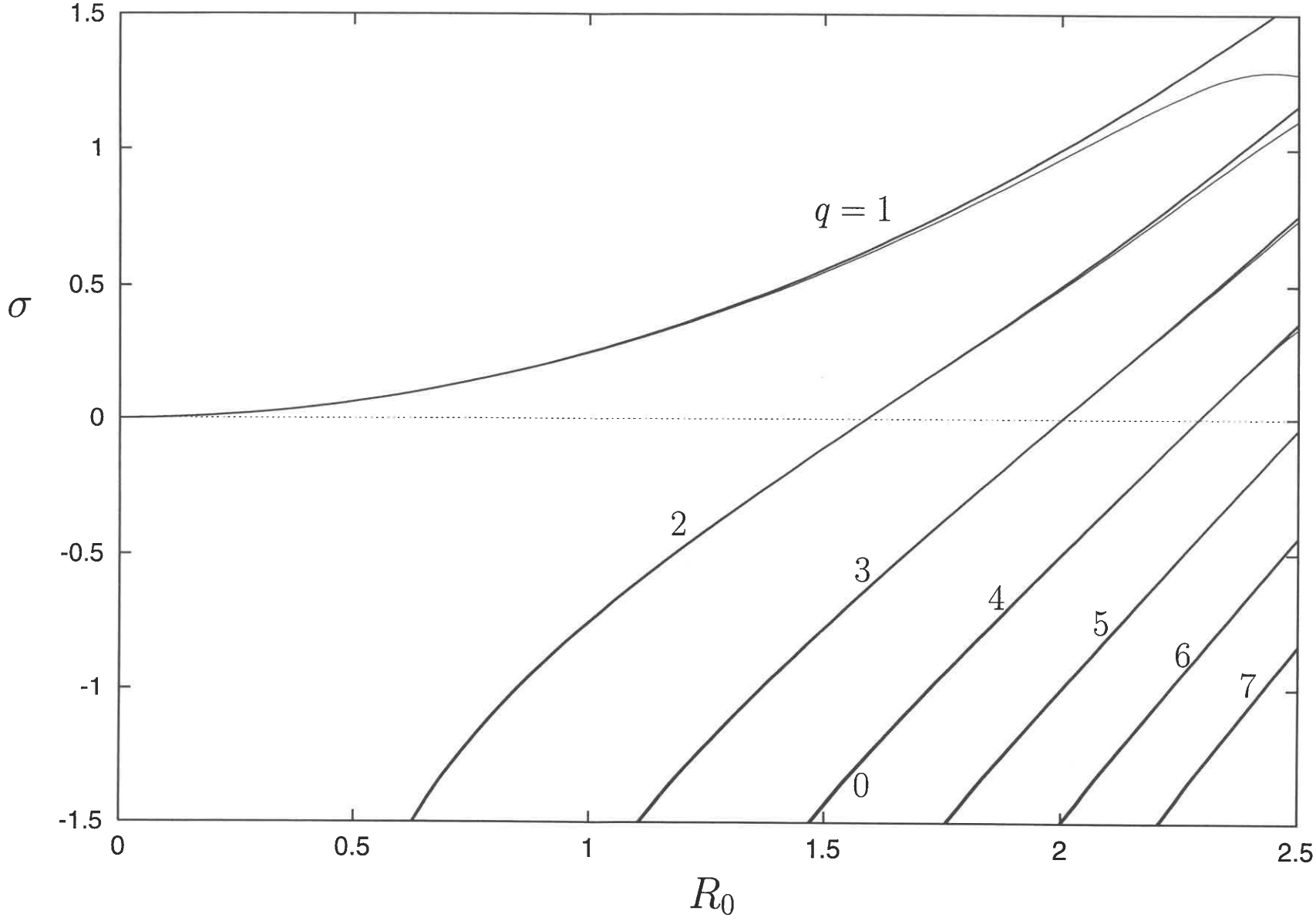

Figure 6

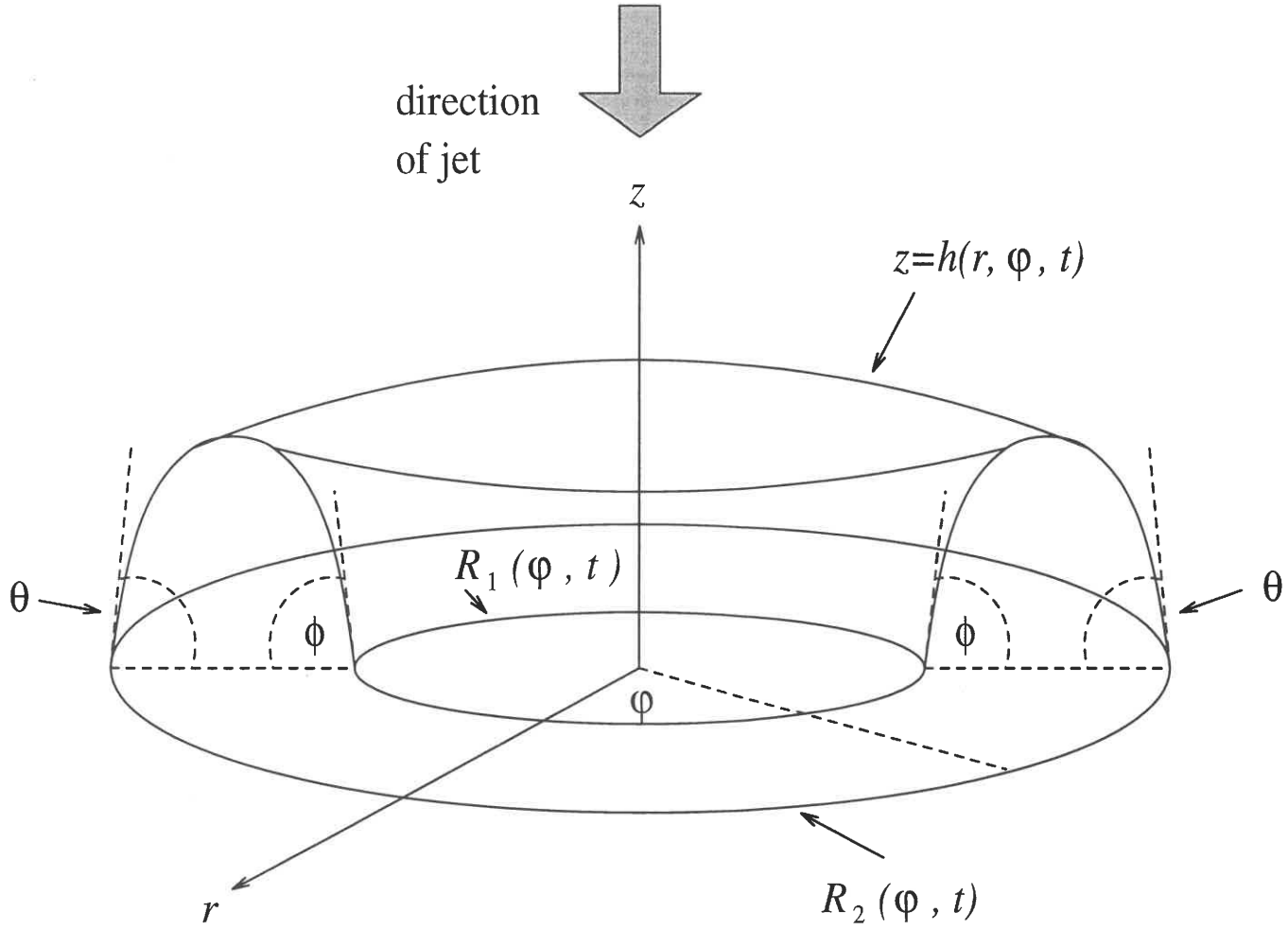

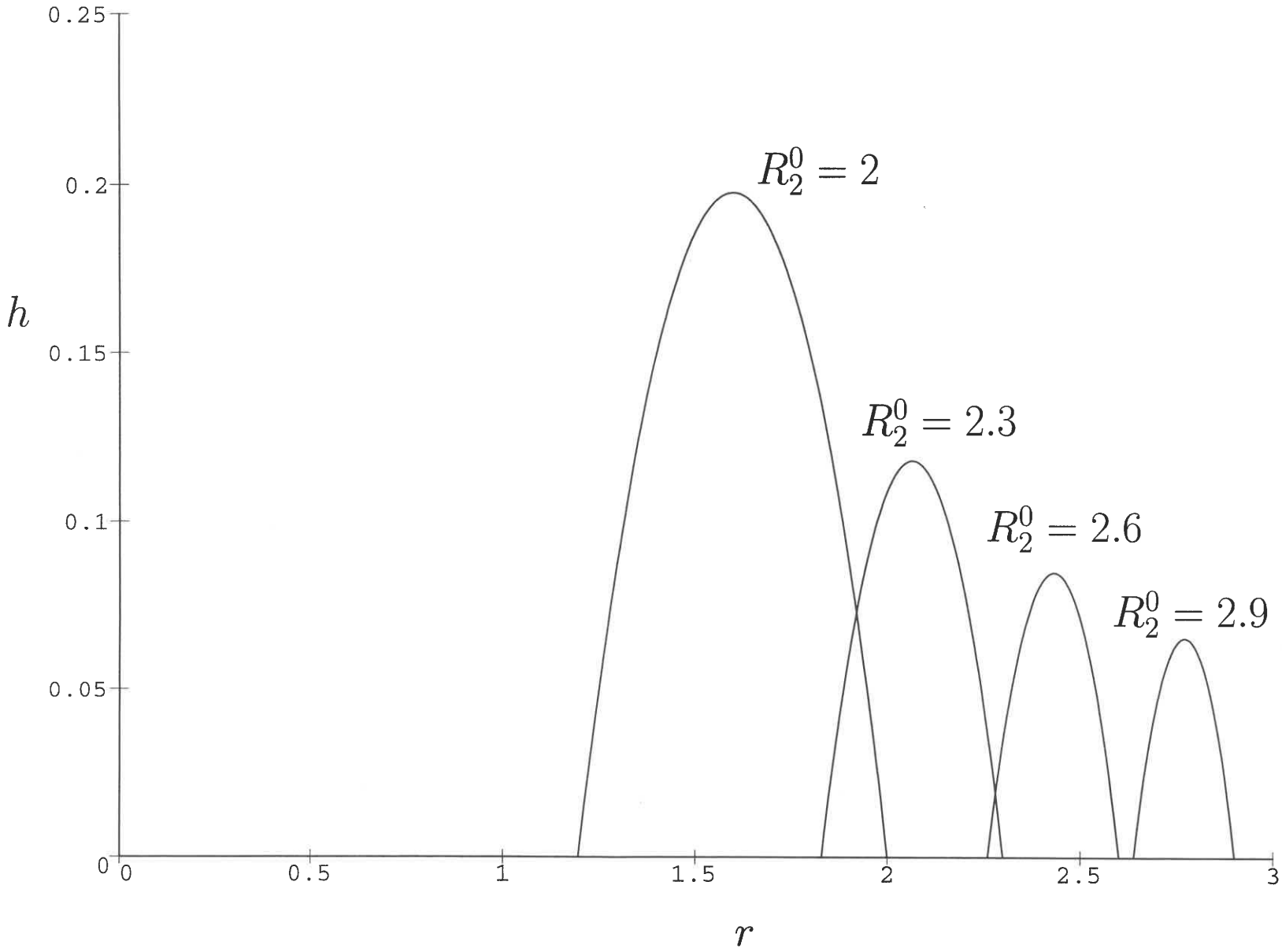
0.25
0.2
0.15
0.1
0.05
0
h
0
0.5
1
1.5
2
2.5
3
r
$R_2^0 = 2$
$R_2^0 = 2.3$
$R_2^0 = 2.6$
$R_2^0 = 2.9$

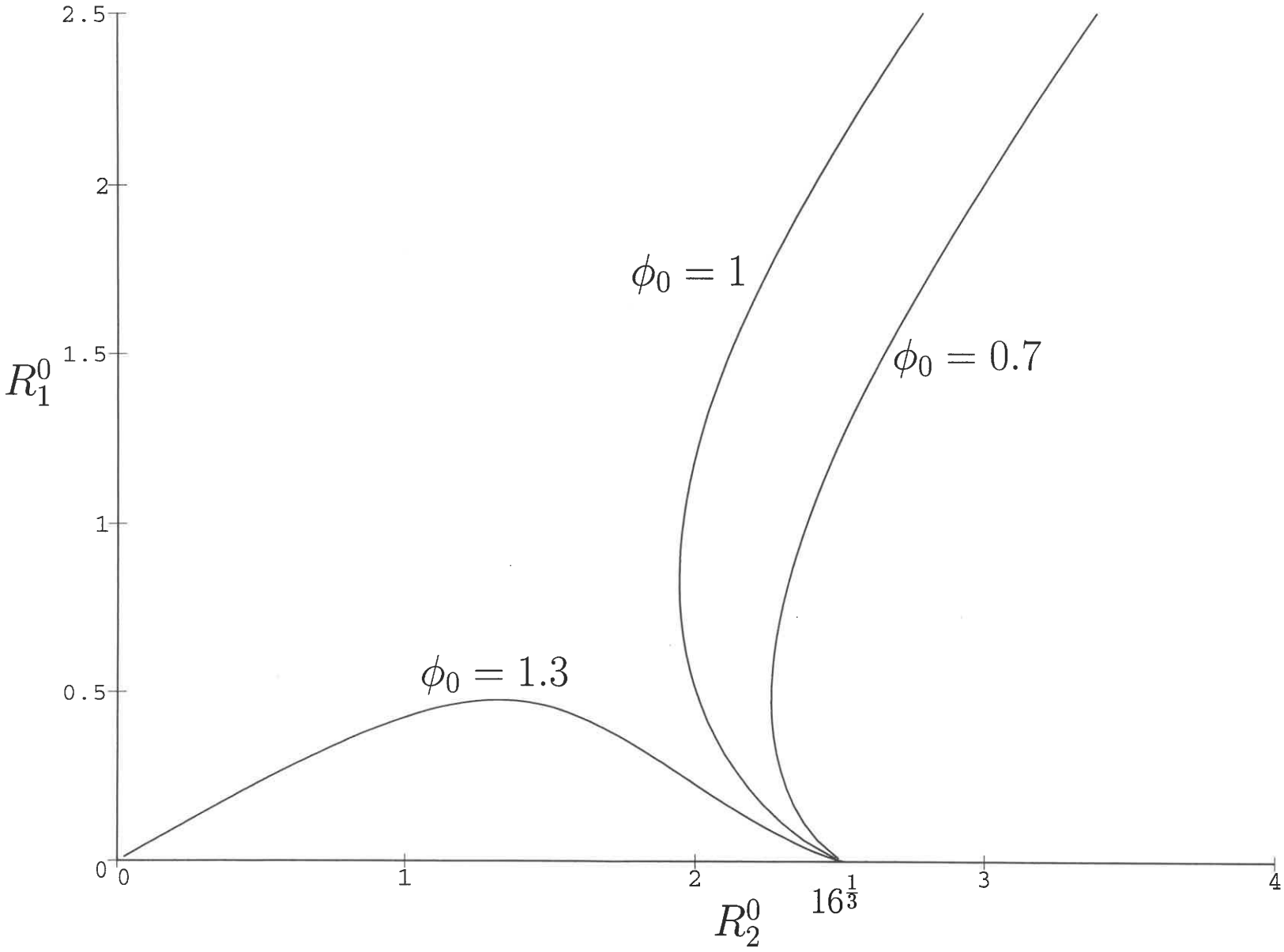
2.5
2
1.5
1
0.5
0
R_1^0
$\phi_0 = 1$
$\phi_0 = 0.7$
$\phi_0 = 1.3$
0
1
2
$16^{\frac{1}{3}}$
3
4
R_2^0

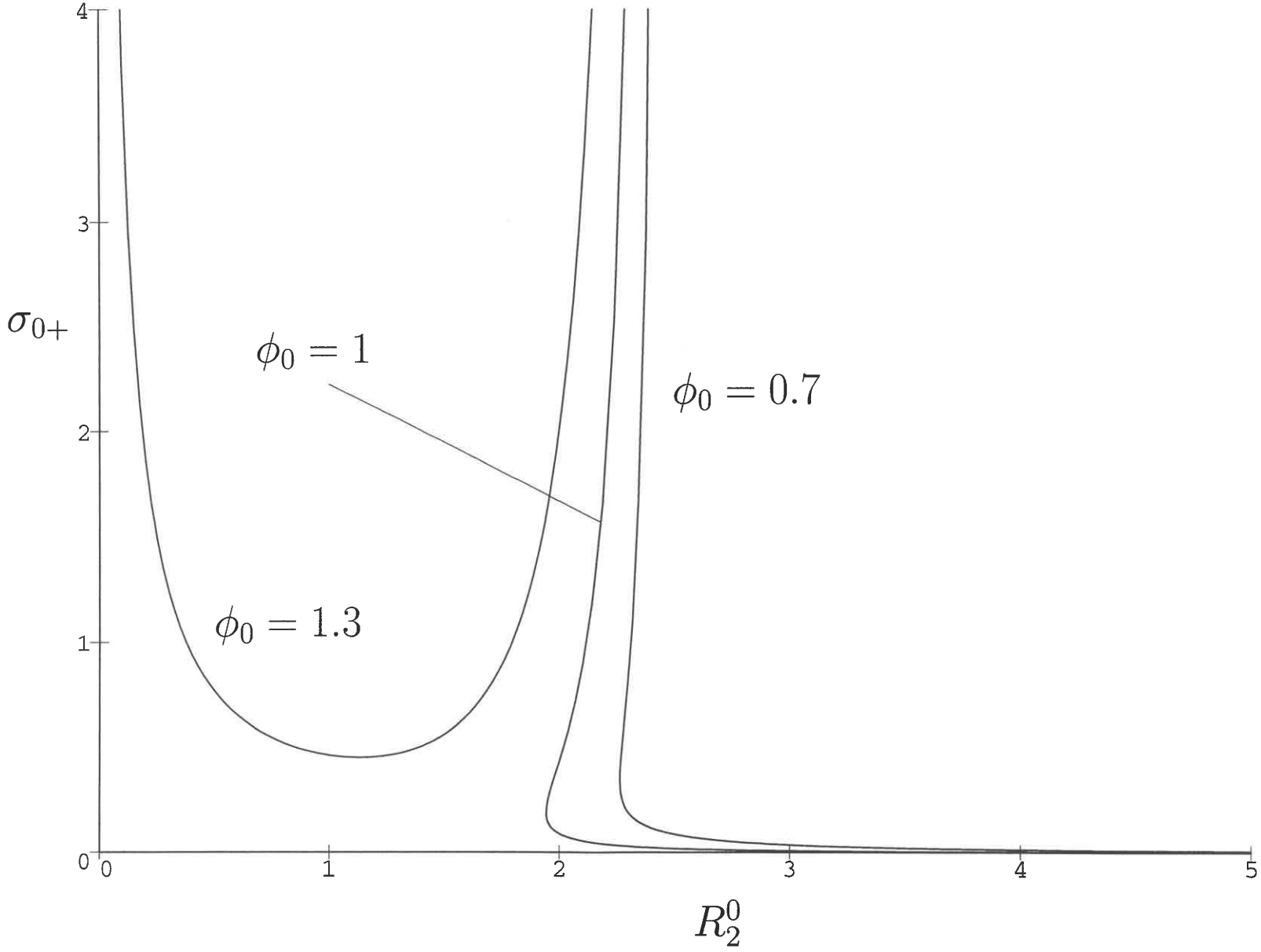
σ_{0+}
$\phi_0 = 1$
$\phi_0 = 0.7$
$\phi_0 = 1.3$
0
1
2
3
4
5
R_2^0

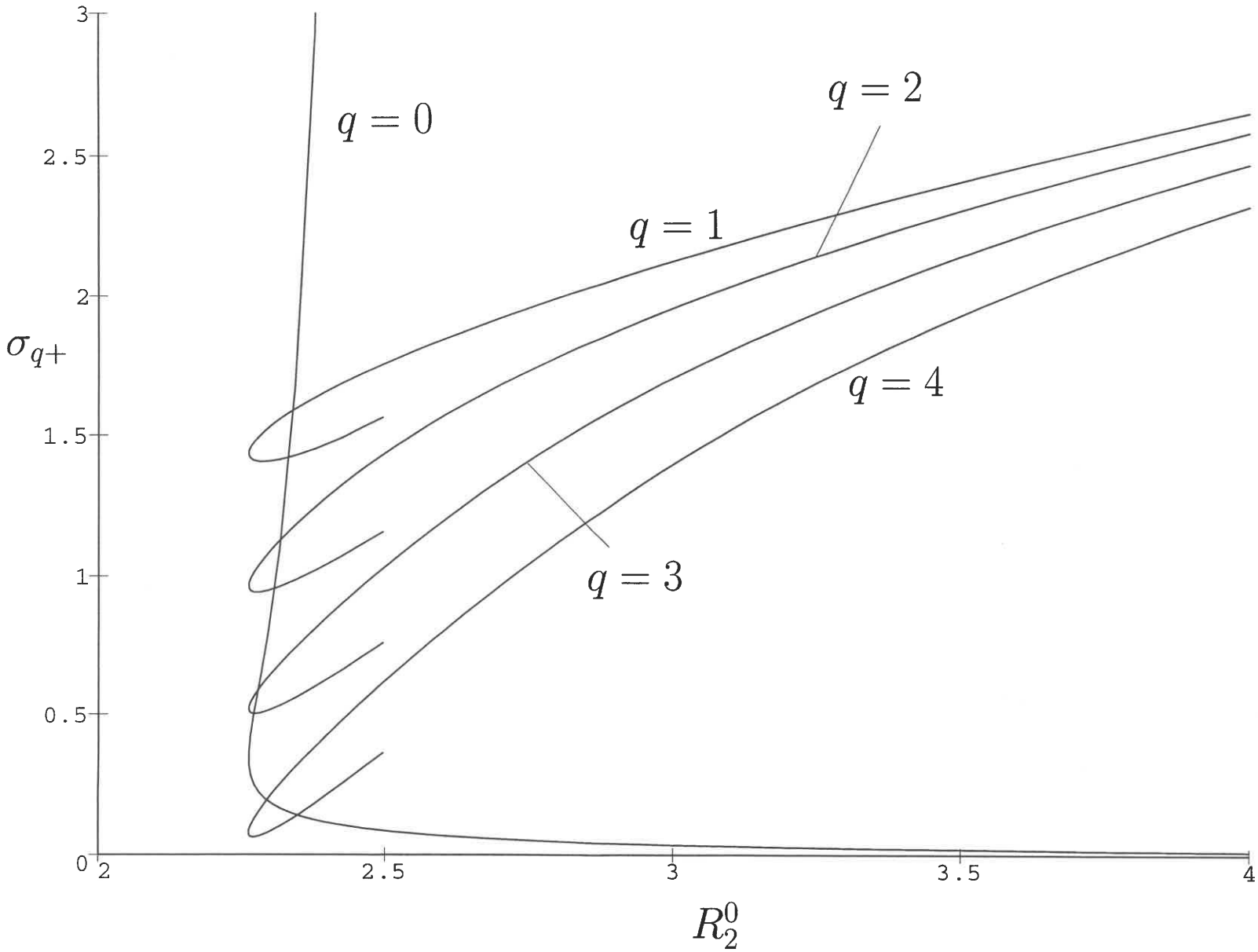
3
2.5
2
1.5
1
0.5
0
2
2.5
3
3.5
4
σ_{q+}
R_2^0
$q = 0$
$q = 1$
$q = 2$
$q = 3$
$q = 4$

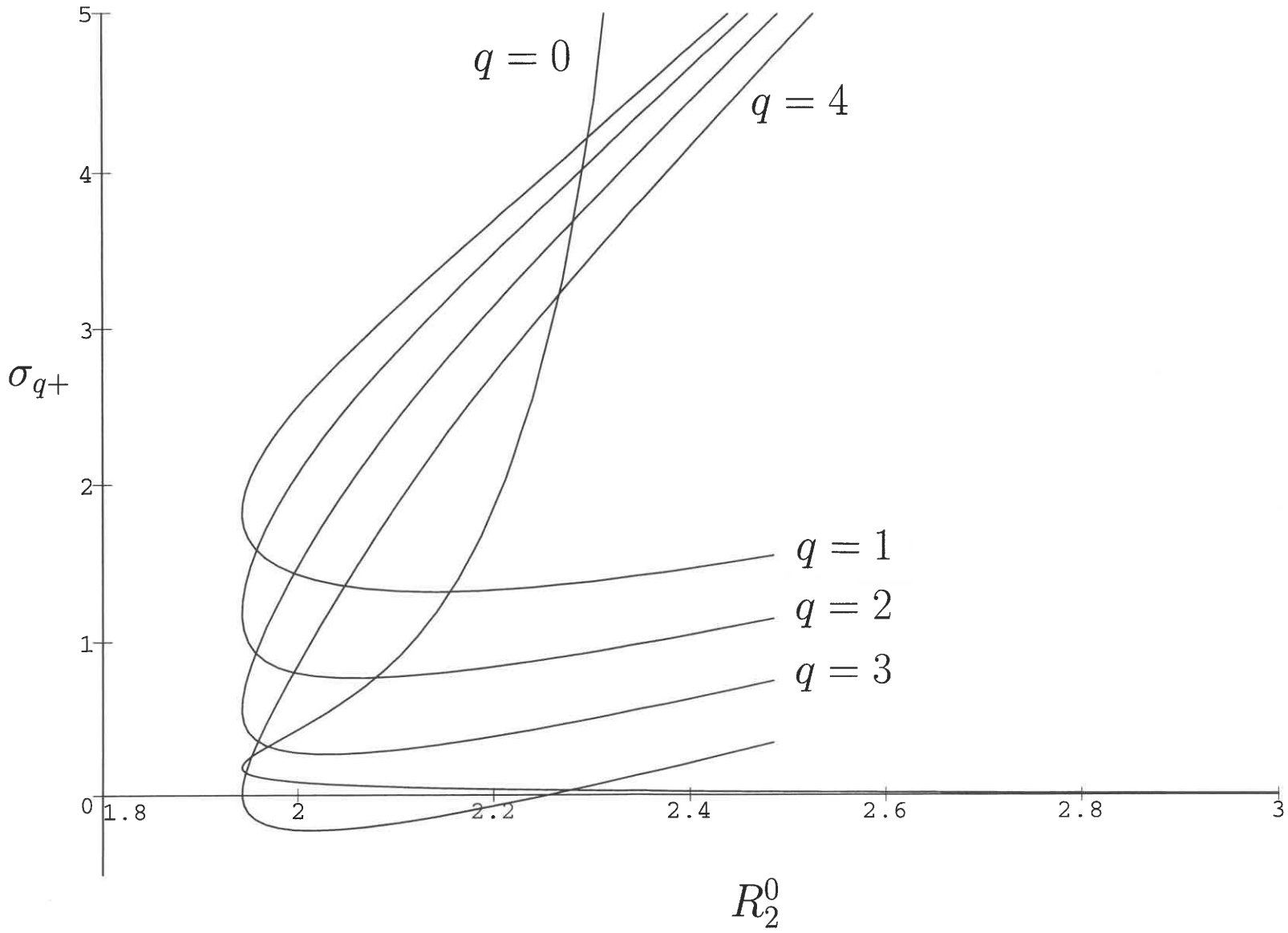
$q = 0$
$q = 4$
$q = 1$
$q = 2$
$q = 3$
σ_{q+}
R_2^0
0
1
2
3
4
5
1.8
2
2.2
2.4
2.6
2.8
3

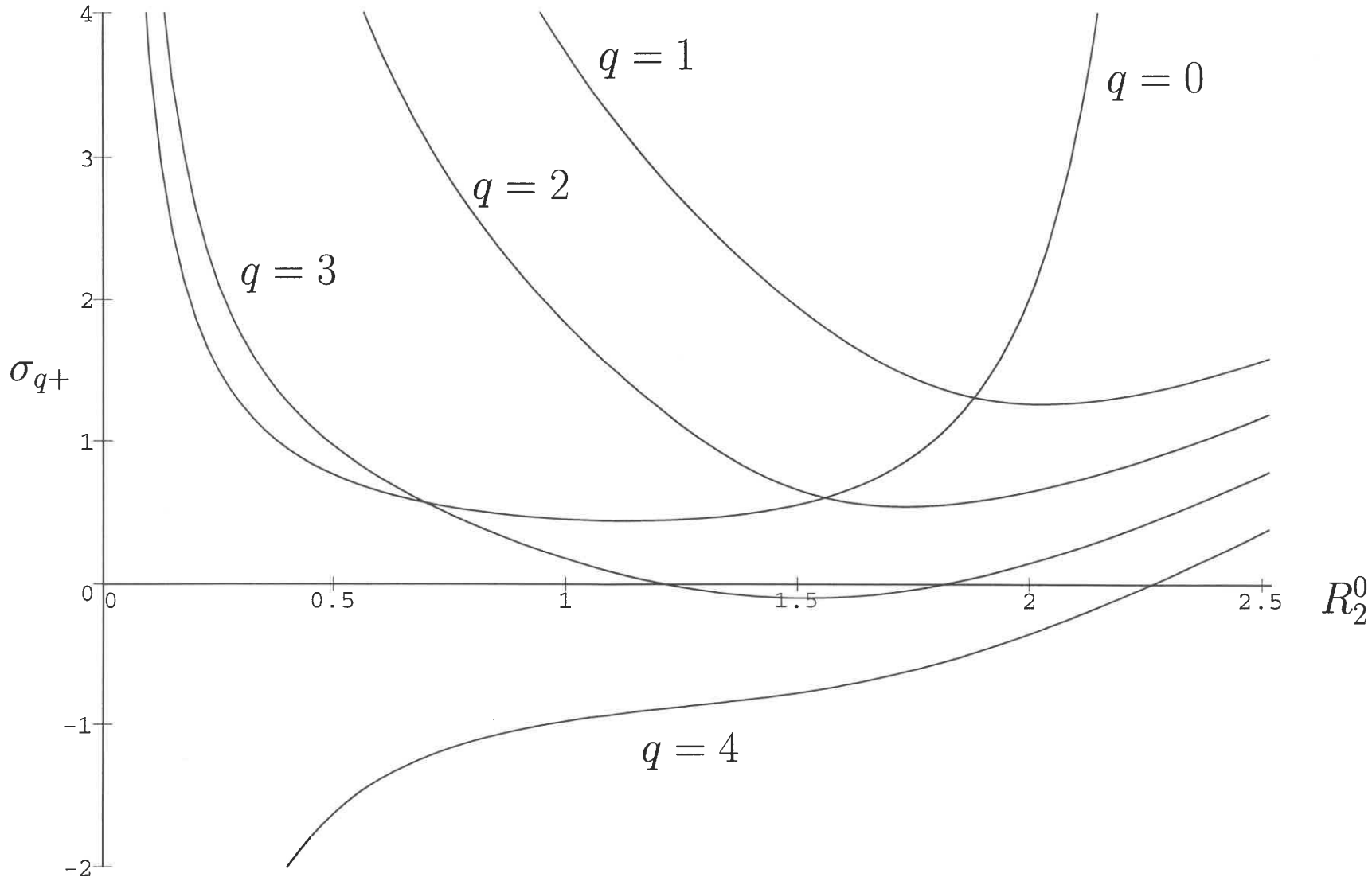
$q = 1$
$q = 0$
$q = 2$
$q = 3$
$q = 4$
σ_{q+}
R_2^0
4
3
2
1
0
-1
-2
0
0.5
1
1.5
2
2.5

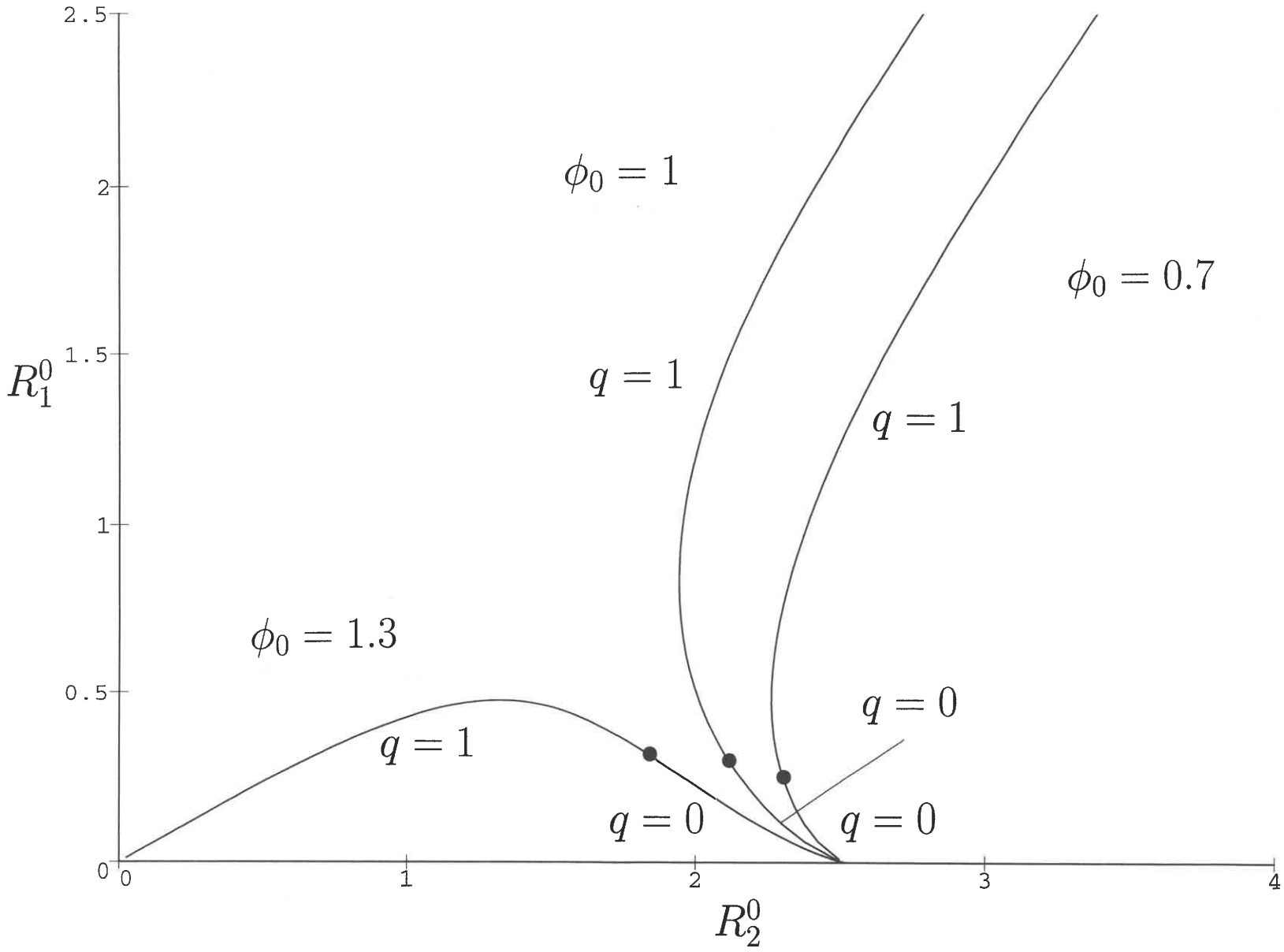
2.5
2
1.5
1
0.5
0
0
1
2
3
4
R_1^0
R_2^0
$\phi_0 = 1$
$\phi_0 = 0.7$
$\phi_0 = 1.3$
$q = 1$
$q = 1$
$q = 1$
$q = 0$
$q = 0$
$q = 0$

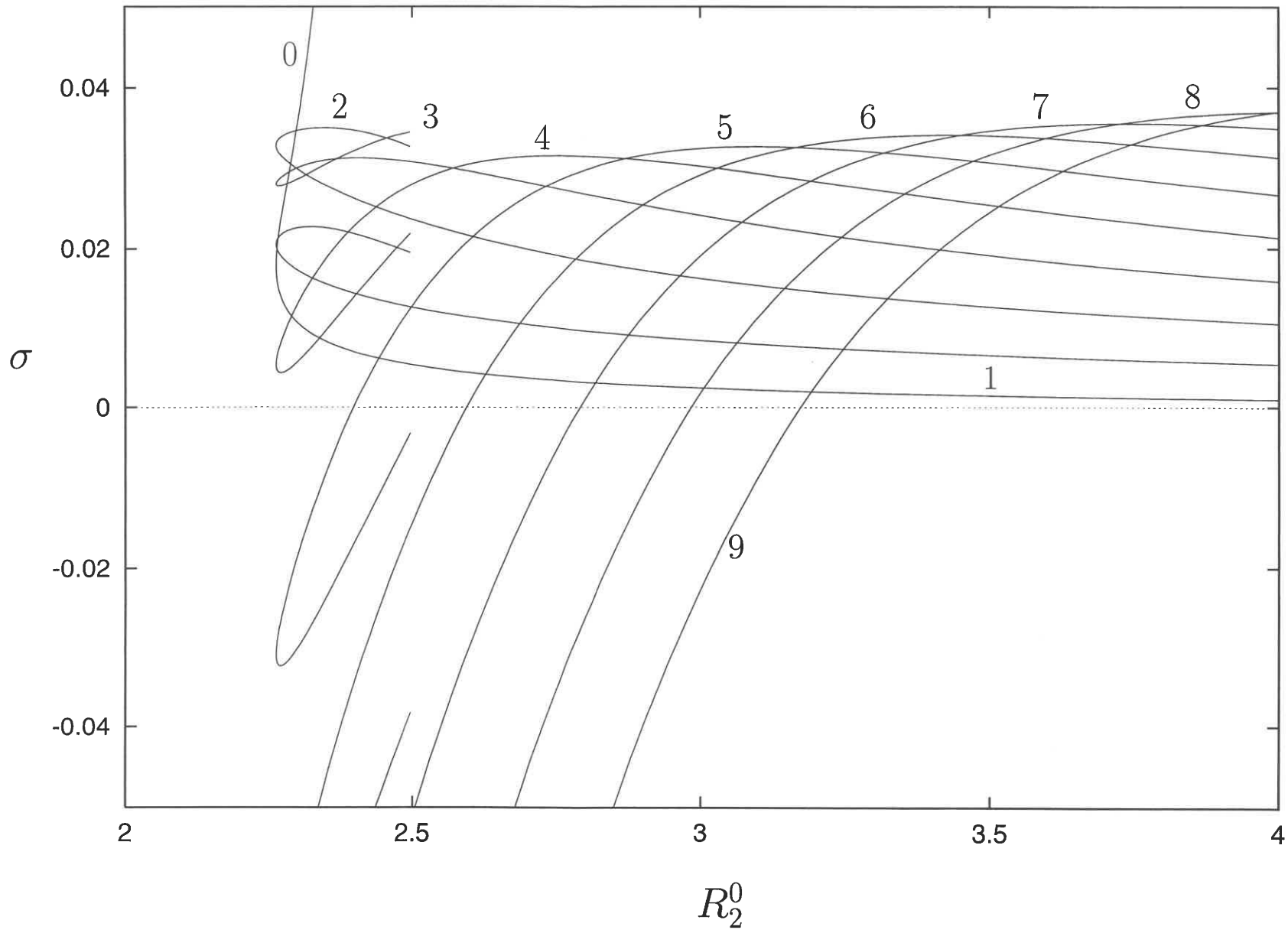
0.04
0.02
0
-0.02
-0.04
σ
2
2.5
3
3.5
4
R_2^0
0
1
2
3
4
5
6
7
8
9

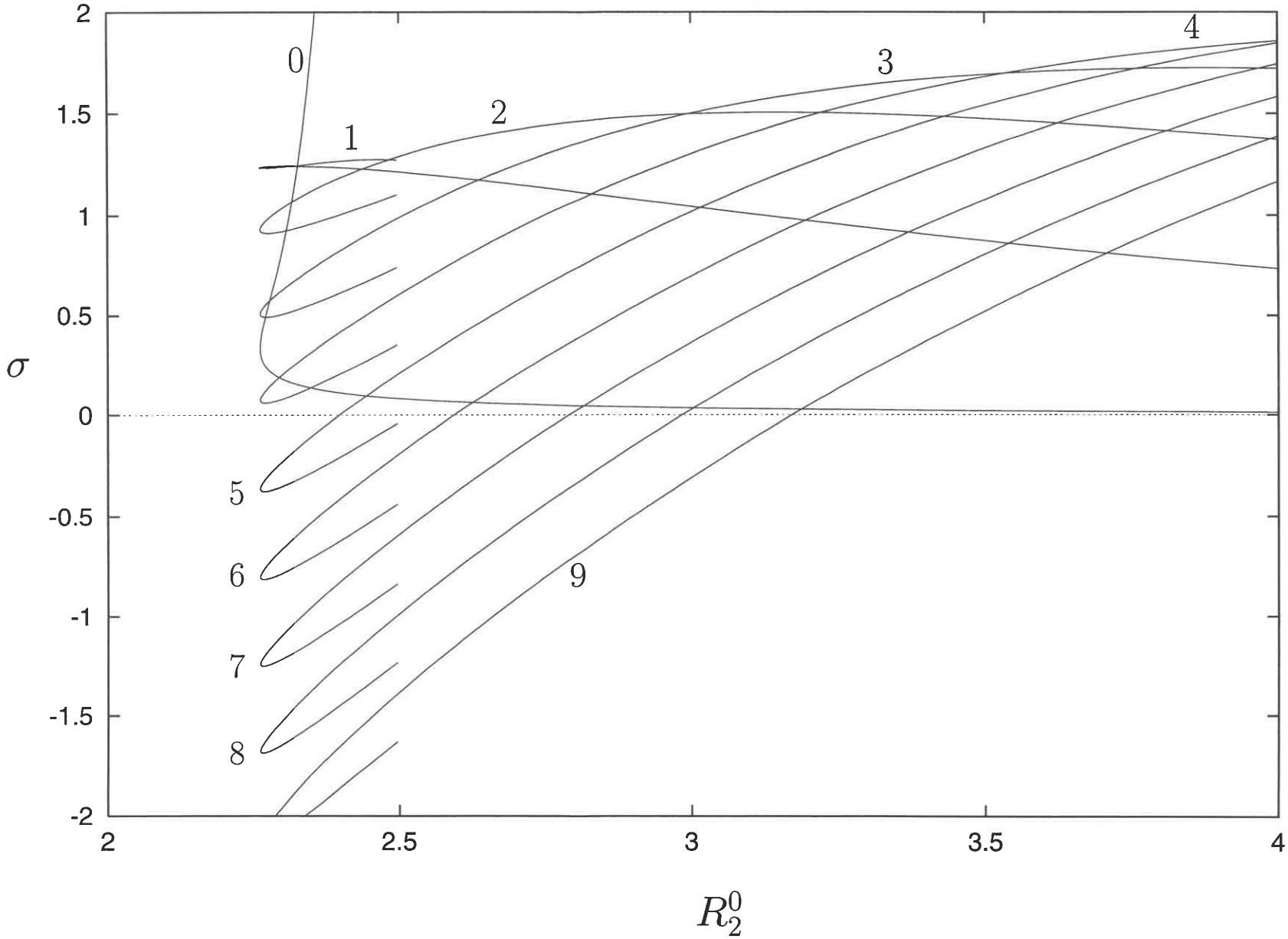
2
1.5
1
0.5
0
-0.5
-1
-1.5
-2
σ
2
2.5
3
3.5
4
R_2^0
0
1
2
3
4
5
6
7
8
9

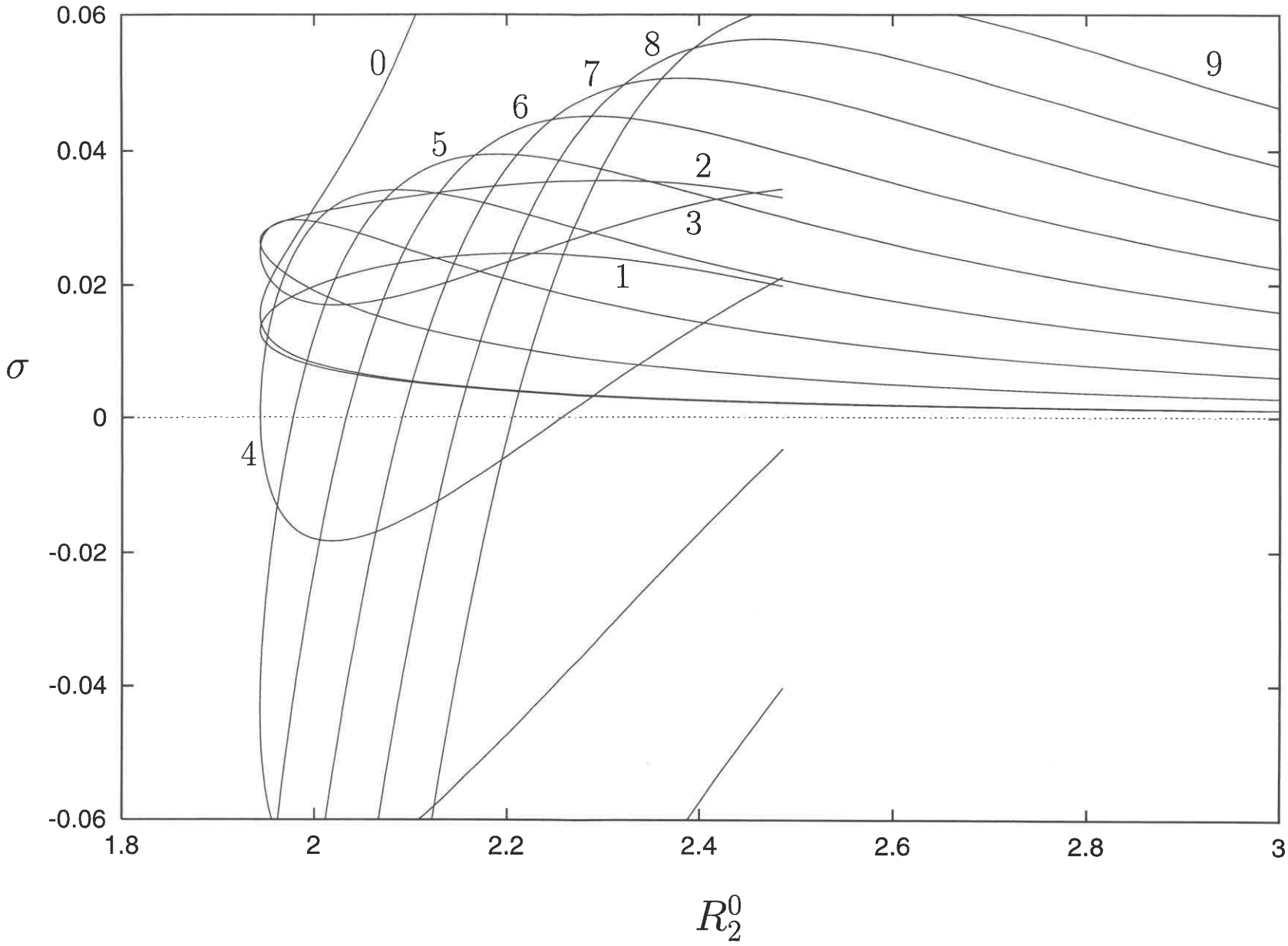
0.06
0.04
0.02
0
-0.02
-0.04
-0.06
σ
1.8
2
2.2
2.4
2.6
2.8
3
R_2^0
0
1
2
3
4
5
6
7
8
9

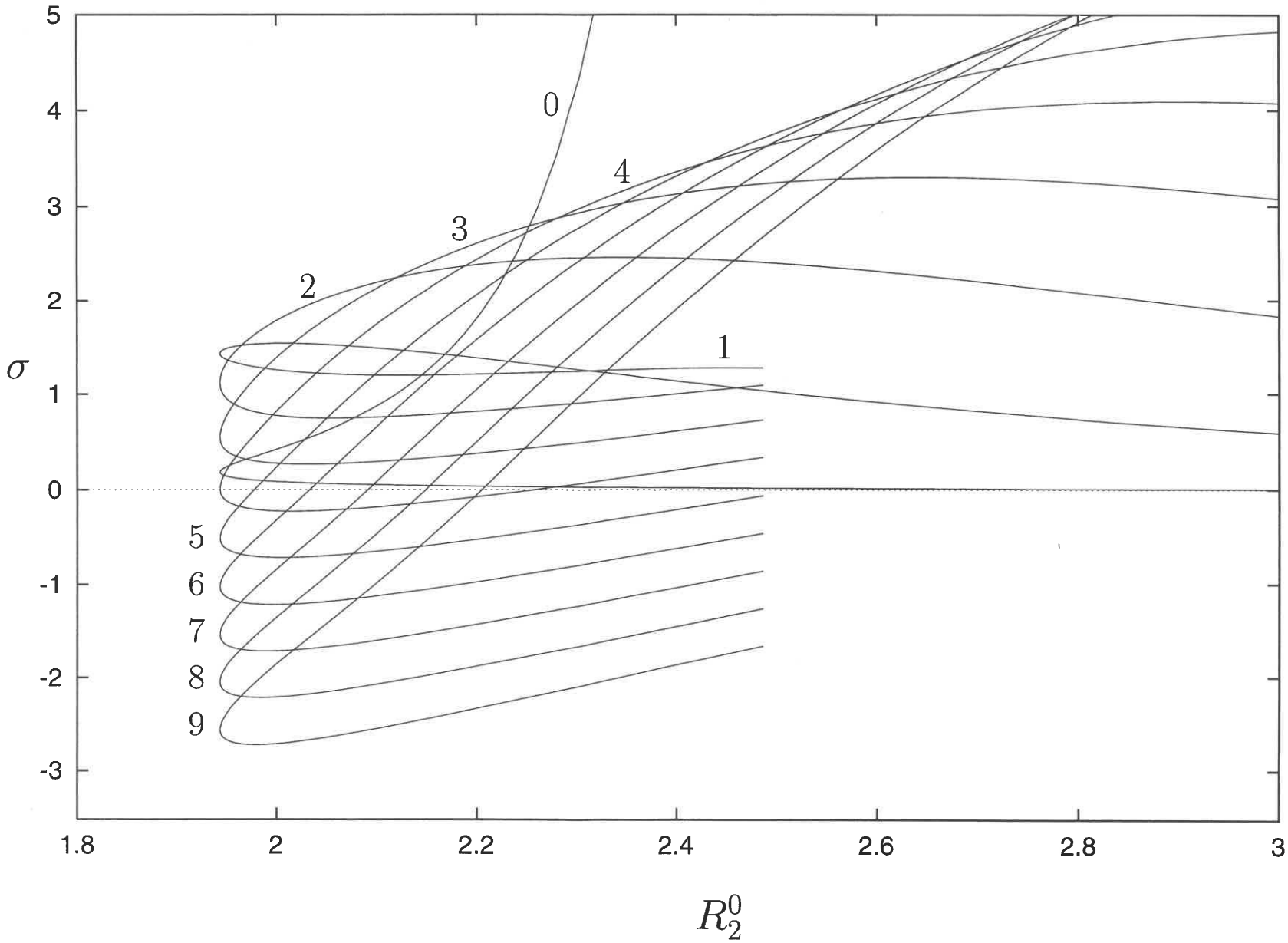
5
4
3
2
1
0
-1
-2
-3
σ
1.8
2
2.2
2.4
2.6
2.8
3
R_2^0
0
1
2
3
4
5
6
7
8
9

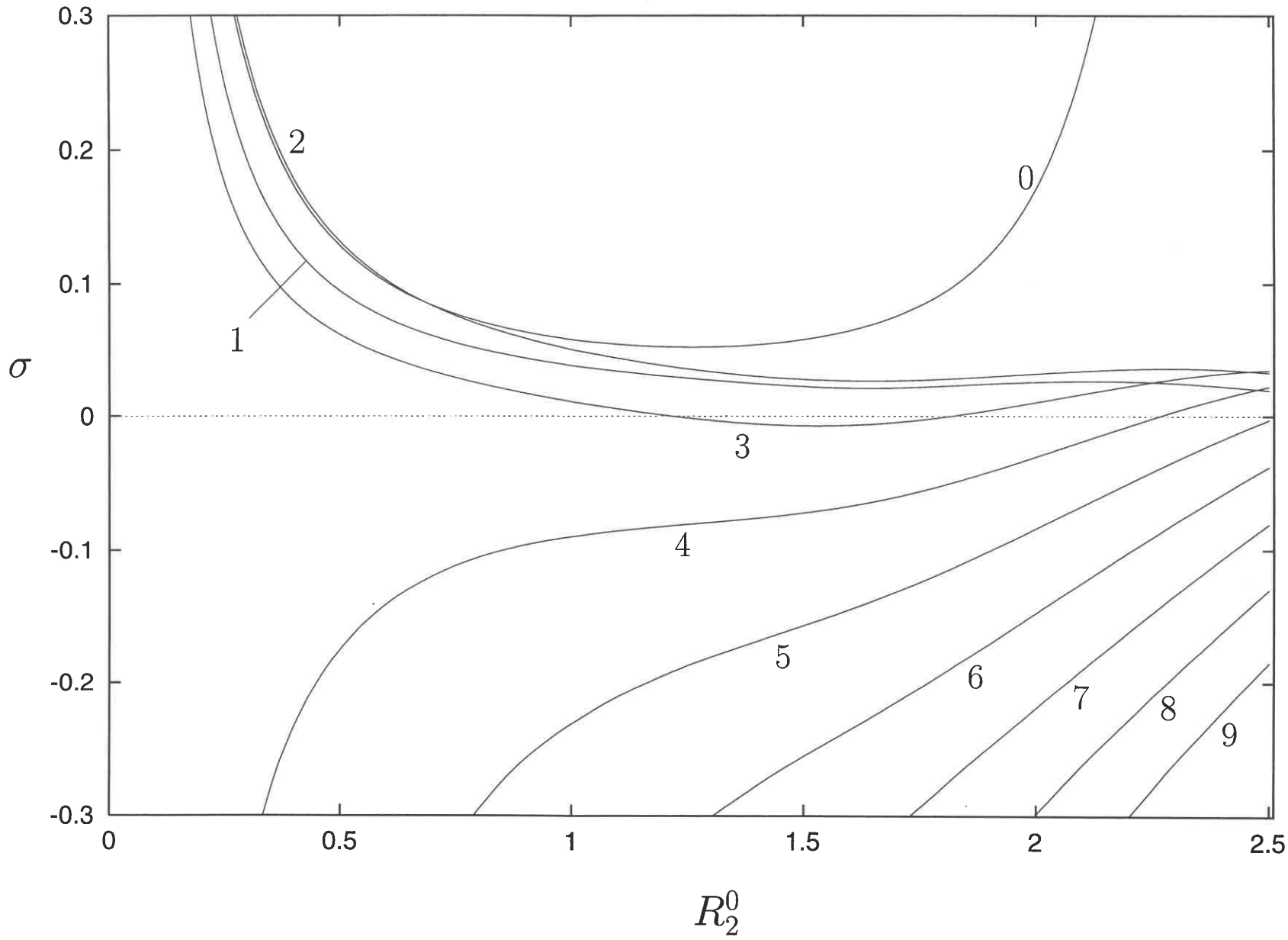
0.3
0.2
0.1
0
-0.1
-0.2
-0.3
σ
0
0.5
1
1.5
2
2.5
R_2^0
0
1
2
3
4
5
6
7
8
9

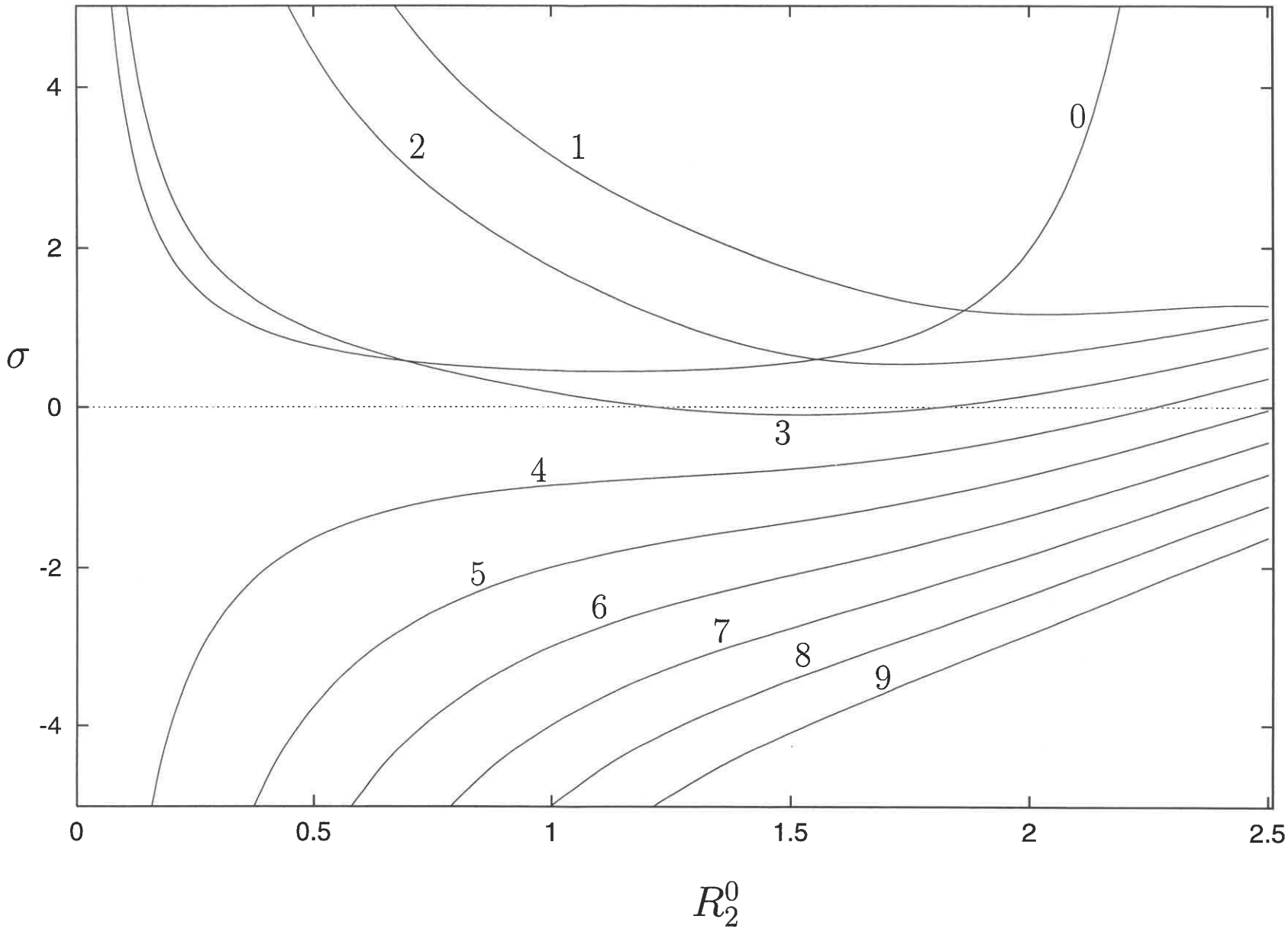
4
2
0
-2
-4
σ
0
0.5
1
1.5
2
2.5
R_2^0
0
1
2
3
4
5
6
7
8
9

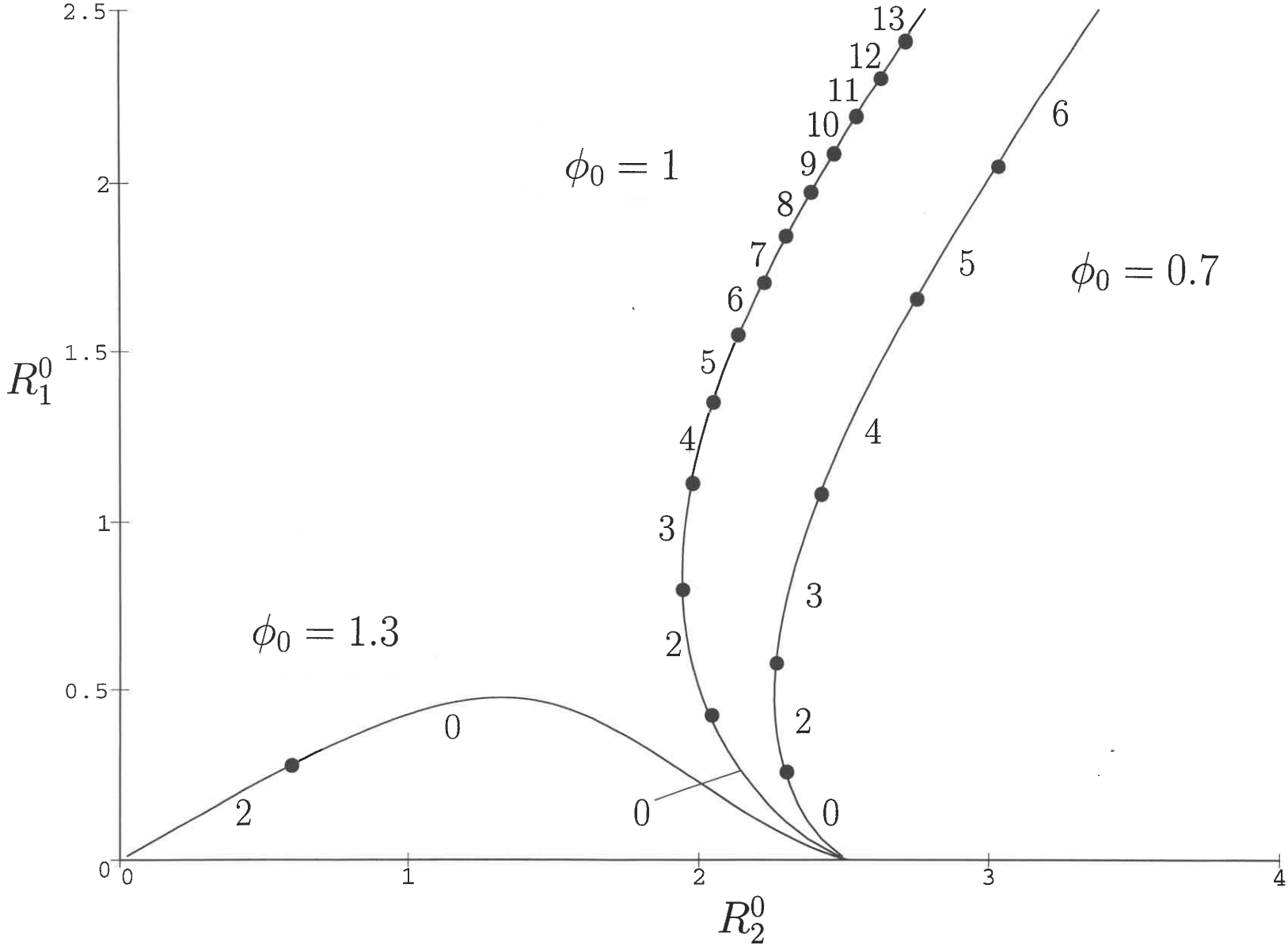
2.5
2
1.5
1
0.5
0
0
1
2
3
4
R_1^0
R_2^0
$\phi_0 = 1$
$\phi_0 = 0.7$
$\phi_0 = 1.3$
13
12
11
10
9
8
7
6
5
4
3
2
1
0
6
5
4
3
2
1
0
2
0
0

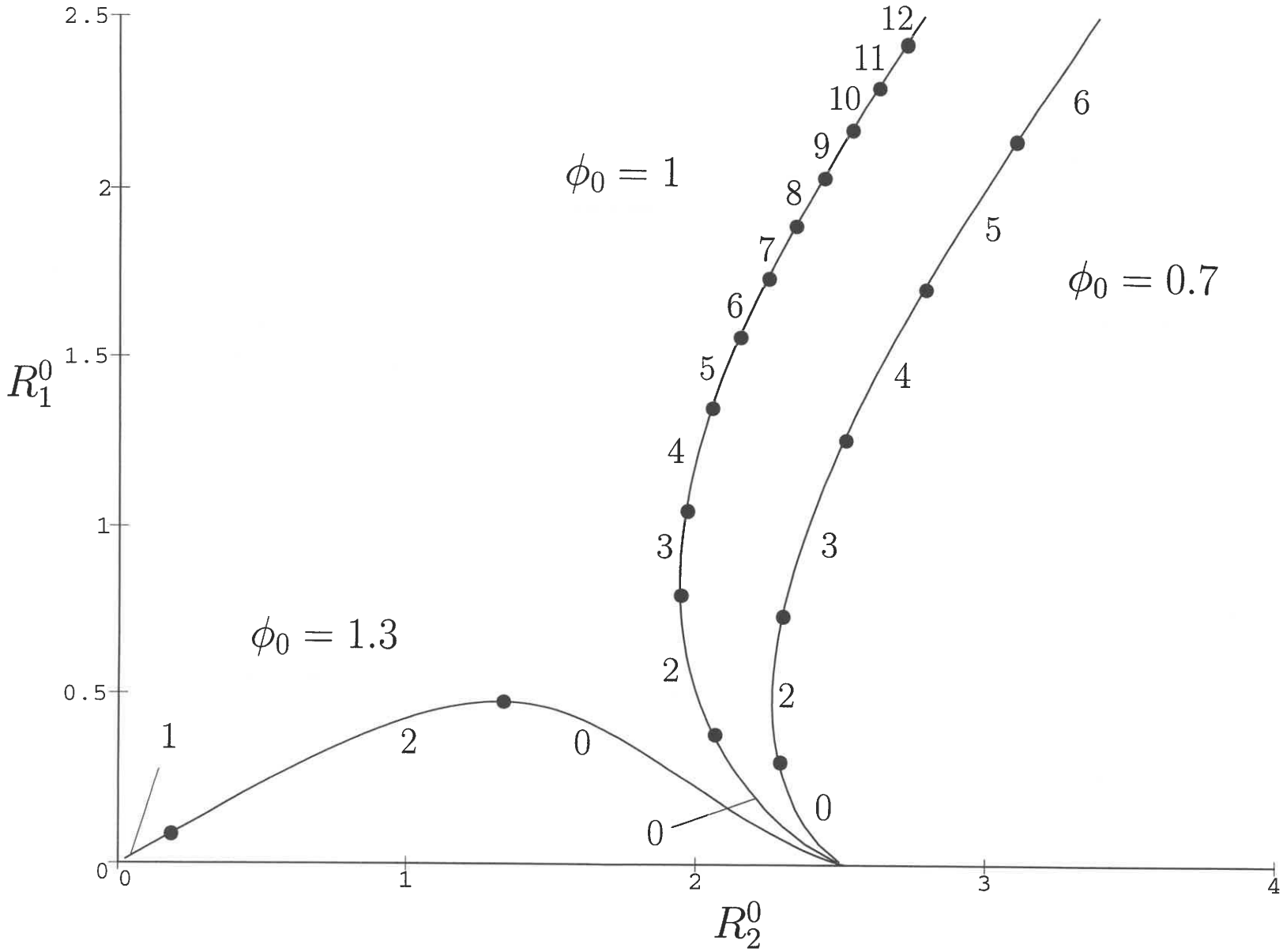
2.5
2
1.5
1
0.5
0
0
1
2
3
4
R_1^0
R_2^0
$\phi_0 = 1$
$\phi_0 = 0.7$
$\phi_0 = 1.3$
12
11
10
9
8
7
6
5
4
3
2
1
0
6
5
4
3
2
0
1
2
0
0

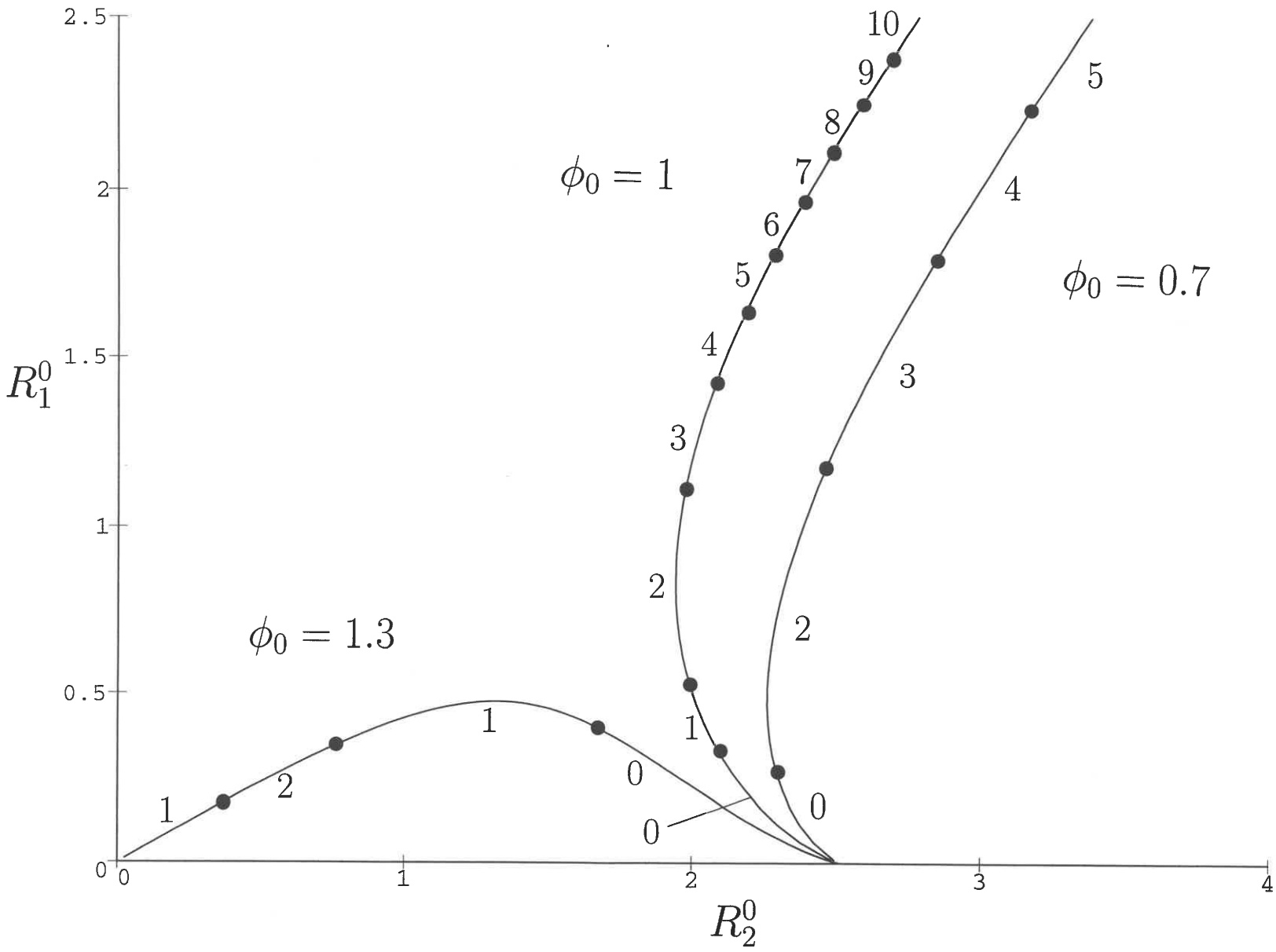
$\phi_0 = 1$
$\phi_0 = 0.7$
$\phi_0 = 1.3$
R_1^0
R_2^0
2.5
2
1.5
1
0.5
0
0
1
2
3
4

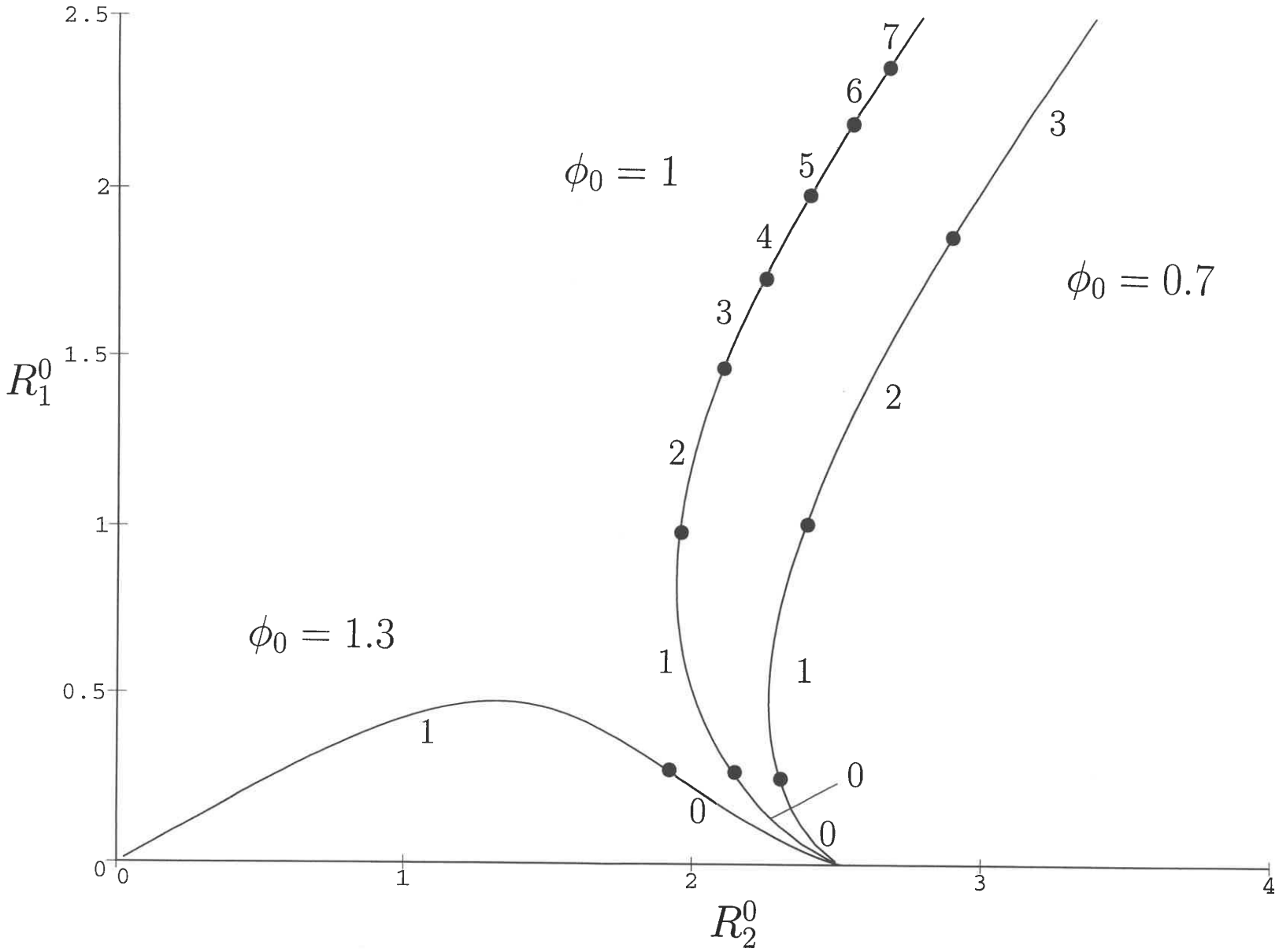
2.5
2
1.5
1
0.5
0
0
1
2
3
4
R_1^0
R_2^0
$\phi_0 = 1$
$\phi_0 = 0.7$
$\phi_0 = 1.3$
7
6
5
4
3
2
1
0
3
2
1
0
1
0
0